Journal of Physics A:
Mathematical and
Theoretical

Transition path properties of a run and tumble particle subjected to an external potential

To cite this article before publication: Hua Li *et al* 2025 *J. Phys. A: Math. Theor.* in press https://doi.org/10.1088/1751-8121/ade5db

Transition path properties of a run and tumble particle subjected to an external potential

Hua Li,[1] Yong Xu,[2,3,*] Ralf Metzler,[4,5,†] Zhanqing Wang,[6] and Kheder Suleiman[2]

[1] *School of Mathematics and Statistics, North China University of Water Resources and Electric Power, Zhengzhou, 450046, China*
[2] *Department of Applied Mathematics, Northwestern Polytechnical University, Xi'an, 710072, China*
[3] *MOE Key Laboratory for Complexity Science in Aerospace, Northwestern Polytechnical University, Xi'an, 710072, China*
[4] *Institute of Physics & Astronomy, University of Potsdam, 14476 Potsdam, Germany*
[5] *Asia Pacific Centre for Theoretical Physics, Pohang 37673, Republic of Korea*
[6] *School of Science, Xi'an University of Architecture and Technology, Xi'an 710055, China*

(Dated: May 29, 2025)

Run-and-tumble particle (RTP) motion is a key model for certain bacteria and other actively moving microscopic particles, combining phases of directed motion with "tumbles", stationary phases during which the particle reorients itself. We here continue previous studies of unconstrained RTP motion and consider the transition path properties of an RTP subjected to an external potential. Exact expressions are derived for the RTP transition path properties, supported by results from Monte Carlo simulations. We explore the effects of particle velocity, tumble rate and the external potential on the splitting probability, transition path time, coefficient of variation, transition path shape, unsuccessful transition path distribution and duration, based on forward and backward master equations. Counterintuitively, the presence of the potential may accelerate the escape of RTPs. Moreover, we show that the external potential gives rise to the appearance of an asymmetry of the transition path properties which increases with the steepness of the potential. While the potential does not affect the forward and reverse transition paths of the RTP, these are affected by the particle velocity, in contrast with free RTPs.

I. INTRODUCTION

Active particle systems [1–4] consume energy and convert it into their own directional motion. The energy may be extracted from the environment or from internal (e.g., biochemical) sources. The range of active systems is very wide, from micro-scale microorganisms such as moving cells and bacteria [5], to the macro-scale including swimming fish, flying birds, or animals migrating on land [6]. In addition to natural active systems, there also exist a growing number of artificial active systems, such as artificial self-driven particles or other active materials [7–9]. Research in active systems aims to understand the complex behaviours and emergent phenomena that arise from the interactions between active particles, with profound implications for physical, biological, materials, and robotics sciences [10–12].

A paradigmatic example of active particles is the run-and-tumble particle (RTP), which is a classic model for describing the intermittent motion governed by phases of directed swimming and direction-changing tumbling. Typical RTPs are bacteria such as Escherichia coli or Bacillus subtilis [13–15]. The movement of RTPs is effected by self-propulsion, e.g., due to flagellar filaments, based on the non-equilibrium conversion of energy, and they exhibit many interesting dynamical phenomena [16]. Special interest has been devoted to the transition properties of RTPs, revealing several remarkable dynamical behaviours different from those observed in equilibrium systems. The study of RTPs splits into two broad categories, studying the motion of RTPs in unconfined environments or when the RTPs move in complex environments with boundaries or obstacles. In the unconfined case the dynamics of RTPs was characterised by quantities such as the position distribution [17–20], the escape/first-passage behaviour [21–23], or the distribution of times required for an RTPs to reach a maximum displacement [24]. However, it is important to unveil the dynamics of RTPs in their natural, complex environments [25]. Understanding the interplay between RTP motion and obstacles as well as boundaries provides relevant clues to bio- and medicine technology applications [26].

Rich behaviours for RTPs in confinement have been uncovered such as the steady state probability density [27–31], entropy production [32–34], random search [35], or first-passage properties [36–39]. An active particle trapped in a confining potential generally has a non-Boltzmann stationary distribution [40, 41]. Interestingly, the probability

*Electronic address: hsux3@nwpu.edu.cn
†Electronic address: rmetzler@uni-potsdam.de (Ralf Metzler, corresponding author)

density of RTPs confined in a box concentrates near the boundaries [42], similar to persistent long-range correlated motion [43]. Here we study another important context of RTPs, their transition path properties, in a finite interval and in the presence of an external potential.

Many processes in chemistry, physics and life sciences, ranging from chemical and enzymatic reactions to transport processes in condensed matter, conformational transformation of macromolecules, protein folding, etc., need a thermal activation to cross some barrier in the relevant coordinates [44, 45]. The transition path is an important concept that describes the real occurrence of thermal activation process and the associated dynamics [46]. Transition path properties mainly include the transition path time [47], the coefficient of variation of the transition path time distribution [48], and the transition path shape [49]. The transition path time [50] is the duration that characterises the real occurrence of thermal activation process, such as, the transit time of cell membrane pores, ion channel transport, or polymer translocation time through a pore [51–55]. The mean transition path time, which is defined as the average time it takes for the particle to move along the transition path from an initial state to a final state, plays an important role in characterising the dynamic behaviour. The transition path shape [56] characterises the temporal and spatial evolution of the distribution of the transition path within the transition region. The coefficient of variation (COV) C_V, the ratio of the standard deviation and the mean of a probability density, is a statistical measure that describes the degree of dispersion of the probability distribution and has also been used to quantify the width of transition path time distributions [57]. For an exponential distribution, $C_V = 1$; when $C_V < 1$ ("low-variance") the distribution is narrower than an exponential distribution, while for $C_V > 1$ ("high-variance") it is broader. We note that the COV is a vital measure for the multidimensionality of the system [58].

Generally, the mean transition path time is calculated solely from successful barrier crossing events, and it is therefore (much) shorter than the mean first-passage time across the same barrier, as the latter also includes (many) unsuccessful ("unproductive") crossing attempts due to the height of the barrier as compared to thermal energy [59]. Indeed, the study of unproductive paths started to emerge [59, 60]. It was shown that unsuccessful paths can provide complementary information not available in the transition path, as these paths explore additional parts of the reaction phase space than transition paths. A crucial example are unsuccessful folding events of proteins leading to misfolded conformations [61–63], that are related to diseases, including Alzheimer's and Parkinson's [65, 66]. The study of unsuccessful paths in protein folding is expected to also provide information on the dynamics in the presence of pathogenic factors. We note that the transition path dynamics of equilibrium systems are better studied both theoretically [67] and numerically [68, 69], while the transition path dynamics of non-equilibrium systems, especially concerning the theoretical aspects, remains somewhat elusive. Recently, we considered the transition path dynamics of free RTPs for active, i.e., non-equilibrium RTPs [70]. We are here extending this study to the case when the RTP is under the influence of an external, confining potential.

Concretely, we here combine analytical derivations and stochastic simulations to quantify the transition path properties of RTPs subjected to an external potential, including the splitting probability, transition path time, the COV, transition path shape, distribution of unproductive attempts, and the average duration of unproductive fluctuations. As remarked above, the study of unsuccessful paths of RTPs is expected to shed additional light on the system, on top of the transition paths.

The paper is organised as follows. We first present the main analytical characteristics of the transition path for an RTP in an external potential in Sec. II. Then, we discuss the concrete results and compare them with Monte Carlo simulations in Sec. III. We draw our conclusions in Sec. IV. Appendix A and B provide analytical expressions and a brief derivation of the backward equations and splitting probability, respectively. Explicit forms of the mean transition path time and the COV are presented in App. C. Two explicit results for the mean return times for the linear potential case are revealed in App. D.

II. TRANSITION PATH PROPERTIES OF A RUN AND TUMBLE PARTICLE

Throughout this paper, we consider a one-dimensional RTP subjected to an external potential. The corresponding Langevin equation reads [38]

$$\frac{dx(t)}{dt} = f(x) + v\sigma(t), \tag{1}$$

where x is the time dependent reaction coordinate and v is the constant speed of the RTP. $\sigma(t) = \pm 1$ represents a dichotomous noise switching between ± 1 with a Poisson rate γ. Here we choose the convention that $\sigma = +1$ defines a right-moving state and $\sigma = -1$ a left-moving state. The rate γ corresponds to the tumbling rate of the RTP. The force acting on the particle is $f(x) = -dV(x)/dx$ in terms of the external potential $V(x)$.

The master equation for the probability density function (PDF) associated with the Langevin dynamic (1) then

reads

$$\frac{\partial P_+(x,t|x_0,\sigma_j)}{\partial t} = -\frac{\partial}{\partial x}\left(f(x)+v\right)P_+(x,t|x_0,\sigma_j) - \gamma\big[P_+(x,t|x_0,\sigma_j) - P_-(x,t|x_0,\sigma_j)\big], \tag{2a}$$

$$\frac{\partial P_-(x,t|x_0,\sigma_j)}{\partial t} = -\frac{\partial}{\partial x}\left(f(x)-v\right)P_-(x,t|x_0,\sigma_j) + \gamma\big[P_+(x,t|x_0,\sigma_j) - P_-(x,t|x_0,\sigma_j)\big], \tag{2b}$$

where the $P_\pm(x,t|x_0,\sigma_j)$ denotes the PDF of particles located at x_0 at time t and state ±1, given the initial state σ_j.

A. Splitting probability

For our analysis we use the transition path region $[x_A, x_B]$, where x_A and x_B are the locations of the absorbing boundaries. $\phi_A^{\sigma_j}(x_0,\sigma_i)$ denotes the probability for a particle to exit through the left-hand boundary x_A in the σ_j-moving state given it was initially at position $x_0 \in [x_A, x_B]$ in the state σ_i. Analogously, $\phi_B^{\sigma_j}(x_0,\sigma_i)$ denotes the exit probability through the right boundary x_B. $\phi_{A/B}^{\pm1}$ are the desired splitting probabilities.

The calculation of the splitting probability is related to the first-passage time density (FPTD) $K(x_{A/B},t|x_0)$ from x_0 to $x_{A/B}$. The nth moment $K^{(n)}(x_{A/B}|x_0)$ of the FPTD is defined as [49]

$$K^{(n)}(x_{A/B}|x_0) = \int_0^\infty t^n K(x_{A/B},t|x_0)dt. \tag{3}$$

Similarly, $K^{(n)}(x_{A/B}|x_0,\sigma_j)$ is the nth-order moment of the FPTD of a particle initially located at x_0 in the state σ_j. For the initial velocity we assume that positive and negative particle velocities occur with equal probability (i.e., we consider the symmetric initial velocity condition $\sigma(0) = \pm1$, each with probability 1/2). The "average" nth-order moment $K^{(n)}(x_{A/B}|x_0)$ of the FPTD of a particle initially located at x_0 is then given by

$$K^{(n)}(x_{A/B}|x_0) = \frac{1}{2}\left[K^{(n)}(x_{A/B}|x_0,-1) + K^{(n)}(x_{A/B}|x_0,+1)\right]. \tag{4}$$

Moreover, $K^{(n)}(x_{A/B}|x_0,\sigma_j)$ satisfies the coupled backwards equations [49]

$$\begin{aligned}
-nK^{(n-1)}(x_{A/B}|x_0,+1) &= \left(f(x_0)+v\right)\frac{\partial}{\partial x_0}K^{(n)}(x_{A/B}|x_0,+1) + \gamma\left[K^{(n)}(x_{A/B}|x_0,-1) - K^{(n)}(x_{A/B}|x_0,+1)\right],\\
-nK^{(n-1)}(x_{A/B}|x_0,-1) &= \left(f(x_0)-v\right)\frac{\partial}{\partial x_0}K^{(n)}(x_{A/B}|x_0,-1) + \gamma\left[K^{(n)}(x_{A/B}|x_0,+1) - K^{(n)}(x_{A/B}|x_0,-1)\right],
\end{aligned} \tag{5}$$

with the boundary conditions

$$\begin{aligned}
K^{(n)}(x_A|x_A,-1) = K^{(n)}(x_A|x_B,+1) = 0,\\
K^{(n)}(x_B|x_B,+1) = K^{(n)}(x_B|x_A,-1) = 0.
\end{aligned} \tag{6}$$

We present the derivation of Eq. (5) in Appendix A. Moreover, the zeroth moment of the FPTD is the splitting probability ($\phi_{A/B}(x_0) = K^{(0)}(x_{A/B}|x_0) = \int_0^\infty K(x_{A/B},t|x_0)dt$, in fact, $\int_0^\infty K(x_A,t|x_0)dt + \int_0^\infty K(x_B,t|x_0)dt = 1$), i.e.

$$\begin{aligned}
\left(f(x_0)+v\right)\frac{\partial}{\partial x_0}\phi_A^{\sigma_j}(x_0,+1) + \gamma\big[\phi_A^{\sigma_j}(x_0,-1) - \phi_A^{\sigma_j}(x_0,+1)\big] = 0,\\
\left(f(x_0)-v\right)\frac{\partial}{\partial x_0}\phi_A^{\sigma_j}(x_0,-1) + \gamma\big[\phi_A^{\sigma_j}(x_0,+1) - \phi_A^{\sigma_j}(x_0,-1)\big] = 0,
\end{aligned} \tag{7}$$

and the associated boundary conditions are

$$\begin{aligned}
\phi_A^{+1}(x_A,-1) = 1, \phi_A^{+1}(x_B,+1) = 0,\\
\phi_A^{-1}(x_A,-1) = 1, \phi_A^{-1}(x_B,+1) = 0.
\end{aligned} \tag{8}$$

Without loss of generality, we define $\rho_A(x_0) = \phi_A^{-1}(x_0,+1) + \phi_A^{-1}(x_0,-1)$, and $\mu_A(x_0) = \phi_A^{-1}(x_0,+1) - \phi_A^{-1}(x_0,-1)$. Then, substituting $\rho_A(x_0)$ and $\mu_A(x_0)$ into Eq. (7) results in

$$\begin{aligned}
f(x_0)\frac{\partial}{\partial x_0}\rho_A(x_0) + v\frac{\partial}{\partial x_0}\mu_A(x_0) = 0,\\
f(x_0)\frac{\partial}{\partial x_0}\mu_A(x_0) + v\frac{\partial}{\partial x_0}\rho_A(x_0) - 2\gamma\mu_A(x_0) = 0.
\end{aligned} \tag{9}$$

According to the boundary conditions Eq. (8), we obtain

$$\begin{aligned}\phi_A^{-1}(x_0,-1) &= -C_1\int_{x_A}^{x_0}\frac{\gamma v}{f^2(x)-v^2}N_1(x)dx+\frac{C_2}{2}+\frac{C_2}{2}N_1(x_0),\\ \phi_A^{-1}(x_0,+1) &= -C_1\int_{x_A}^{x_0}\frac{\gamma v}{f^2(x)-v^2}N_1(x)dx+\frac{C_2}{2}-\frac{C_2}{2}N_1(x_0),\end{aligned} \tag{10}$$

where $N_1(x_0)=\exp\left(-\int_{x_0}^{x_B}\frac{2\gamma f(y)}{f^2(y)-v^2}dy\right)$, $C_2=2+C_1N_1(x_A)$, $C_1=-1/\left(-\int_{x_A}^{x_B}\frac{\gamma v}{f^2(x)-v^2}N_1(x)dx+\frac{1}{2}N_1(x_A)+\frac{1}{2}\right)$.

Similarly, combining Eqs. (7) and (8) we obtain

$$\begin{aligned}\phi_A^{+1}(x_0,-1) &= C_3\int_{x_0}^{x_B}\frac{\gamma v}{f^2(x)-v^2}N_2(x)dx+\frac{C_4}{2}+\frac{C_3}{2}N_2(x_0),\\ \phi_A^{+1}(x_0,+1) &= C_3\int_{x_0}^{x_B}\frac{\gamma v}{f^2(x)-v^2}N_2(x)dx+\frac{C_4}{2}-\frac{C_3}{2}N_2(x_0),\end{aligned} \tag{11}$$

which yields

$$\begin{aligned}N_2(x_0) &= \exp\left(\int_{x_A}^{x_0}\frac{2\gamma f(y)}{f^2(y)-v^2}dy\right),\\ C_4 &= -C_3,\quad C_3=\left(\int_{x_A}^{x_B}\frac{\gamma v}{f^2(x)-v^2}N_2(x)dx-\frac{1}{2}N_2(x_B)-\frac{1}{2}\right)^{-1}.\end{aligned} \tag{12}$$

The results for $\phi_B^{\sigma_j}(x_0,\pm1)$ can be obtained in a similar manner, as shown in App. B, where we also derive the results for the special case of a linear potential.

With our assumption of a symmetric initial velocity ($\sigma(0)=\pm1$ each with probability 1/2) above, the "average" splitting probabilities read

$$\begin{aligned}\phi_A^{-1}(x_0) &= \frac{1}{2}[\phi_A^{-1}(x_0,+1)+\phi_A^{-1}(x_0,-1)],\\ \phi_A^{+1}(x_0) &= \frac{1}{2}[\phi_A^{+1}(x_0,+1)+\phi_A^{+1}(x_0,-1)],\\ \phi_A(x_0) &= \frac{1}{2}[\phi_A^{+1}(x_0)+\phi_A^{-1}(x_0)].\end{aligned} \tag{13}$$

Meanwhile,

$$\begin{aligned}\phi_A(x_0,+1) =&\frac{1}{2}[\phi_A^{+1}(x_0,+1)+\phi_A^{-1}(x_0,+1)],\\ \phi_A(x_0,-1) =&\frac{1}{2}[\phi_A^{+1}(x_0,-1)+\phi_A^{-1}(x_0,-1)].\end{aligned} \tag{14}$$

In our notation, $\phi_A^{+1}(x_0)$ and $\phi_A^{-1}(x_0)$ are the splitting probabilities that the particle leaves the transition region at x_A and is in the right-moving (+1) and left-moving (−1) state, respectively. $\phi_A(x_0,+1)$ is the splitting probability of a particle starting from x_0 in the right-moving state and subsequently leaving the transition region through x_A. Similarly, $\phi_A(x_0,-1)$ denotes the case when the particle is initially in the left-moving state. $\phi_B(x_0)$ can be obtained in a similar way.

B. Transition path time and coefficient of variation

We define $\tau^{\mathrm{TP}}(x_B|x_A)$ and $\tau^{\mathrm{TP}}(x_A|x_B)$ as the mean transition path time of the RTP from x_A/x_B to x_B/x_A. $\tau^{\mathrm{TP}}(x_B|x_A)$ is called the forward mean transition path time, and $\tau^{\mathrm{TP}}(x_A|x_B)$ is the reverse case. According to Eq. (5), the first-order moment $K^{(1)}(x_{A/B}|x_0,\pm1)$ of the FPTD satisfies the coupled backward equations

$$\begin{aligned}(f(x_0)+v)\frac{\partial}{\partial x_0}K^{(1)}(x_{A/B}|x_0,+1)+\gamma\left[K^{(1)}(x_{A/B}|x_0,-1)-K^{(1)}(x_{A/B}|x_0,+1)\right] &= -\phi_{A/B}(x_0,+1),\\ (f(x_0)-v)\frac{\partial}{\partial x_0}K^{(1)}(x_{A/B}|x_0,-1)+\gamma\left[K^{(1)}(x_{A/B}|x_0,+1)-K^{(1)}(x_{A/B}|x_0,-1)\right] &= -\phi_{A/B}(x_0,-1).\end{aligned} \tag{15}$$

In order to solve Eq. (15), we define

$$\begin{aligned}\eta_B(x_0) &= K^{(1)}(x_B|x_0,+1)+K^{(1)}(x_B|x_0,-1),\\ \epsilon_B(x_0) &= K^{(1)}(x_B|x_0,+1)-K^{(1)}(x_B|x_0,-1),\end{aligned} \tag{16}$$

with which we immediately obtain

$$\begin{aligned}f(x_0)\frac{\partial}{\partial x_0}\eta_B(x_0)+v\frac{\partial}{\partial x_0}\epsilon_B(x_0) &= -\phi_B(x_0,+1)-\phi_B(x_0,-1),\\ f(x_0)\frac{\partial}{\partial x_0}\epsilon_B(x_0)+v\frac{\partial}{\partial x_0}\eta_B(x_0) &= \phi_B(x_0,-1)-\phi_B(x_0,+1)+2\gamma\epsilon_B(x_0).\end{aligned} \tag{17}$$

For our choice of the potential $V(x)=ax^2+bx+c$, we arrive at the expression

$$\begin{aligned}\epsilon_B(x_0) &= \frac{1}{M_1(x_0)}\int_{x_A}^{x_0}\frac{\phi_B(x,-1)M_1(x)}{f(x)-v}dx-\frac{1}{M_1(x_0)}\int_{x_A}^{x_0}\frac{\phi_B(x,+1)M_1(x)}{f(x)+v}dx+\frac{D_1}{M_1(x_0)},\\ \eta_B(x_0) &= -\int_{x_A}^{x_0}\frac{\phi_B(x,-1)}{f(x)-v}dx-2\gamma v\int_{x_A}^{x_0}\int_{x_A}^{x}\frac{\phi_B(y,-1)M_1(y)}{f(y)-v}dy\frac{dx}{M_1(x)(f^2(x)-v^2)}\\ &\quad -\int_{x_A}^{x_0}\frac{\phi_B(x,+1)}{f(x)+v}dx+2\gamma v\int_{x_A}^{x_0}\int_{x_A}^{x}\frac{\phi_B(y,+1)M_1(y)}{f(y)+v}dy\frac{dx}{M_1(x)(f^2(x)-v^2)}\\ &\quad -2\gamma v D_1\int_{x_A}^{x_0}\frac{dx}{M_1(x)(f^2(x)-v^2)}+D_2,\end{aligned} \tag{18}$$

where

$$M_1(x_0)=\left[\frac{(2ax_B+b)^2-v^2}{(2ax_0+b)^2-v^2}\right]^{\gamma/(2a)}\quad\text{and}\quad D_2=\frac{D_1}{M_1(x_A)}, \tag{19}$$

and where D_1 can be derived via the relation $\eta_B(x_B)+\epsilon_B(x_B)=0$. The form of D_1 is quite complex, and we do not present it here. For the linear potential case, we have presented the detail forms of Eq. (18) in App. B. As a result, we showed how $K^{(1)}(x_B|x_0,+1)=\frac{1}{2}[\epsilon_B(x_0)+\eta_B(x_0)]$ and $K^{(1)}(x_B|x_0,-1)=\frac{1}{2}[\eta_B(x_0)-\epsilon_B(x_0)]$ can be calculated.

The mean first-passage times from the initial position x_0 to x_A/x_B are then given by

$$\tau^{\rm FP}(x_{A/B}|x_0)=\frac{K^{(1)}(x_{A/B}|x_0)}{\phi_{A/B}(x_0)}, \tag{20}$$

where $K^{(1)}(x_{A/B}|x_0)=\frac{1}{2}[K^{(1)}(x_{A/B}|x_0,+1)+K^{(1)}(x_{A/B}|x_0,-1)]$. As x_A and x_B are two absorbing boundaries, the mean transition path times $\tau^{\rm TP}(x_B|x_A)$ and $\tau^{\rm TP}(x_A|x_B)$ can be derived via the limits [49]

$$\begin{aligned}\tau^{\rm TP}(x_B|x_A)&=\tau^{\rm FP}(x_B|x_0\to x_A),\\ \tau^{\rm TP}(x_A|x_B)&=\tau^{\rm FP}(x_A|x_0\to x_B).\end{aligned} \tag{21}$$

We continue with the derivation of the COV C_V of the transition path time distribution. C_V has the form [48]

$$C_V=\frac{\left(\langle t_{\rm TP}^2\rangle-\langle t_{\rm TP}\rangle^2\right)^{1/2}}{\langle t_{\rm TP}\rangle}, \tag{22}$$

in terms of the first and second-order moments of the transition path time distribution, and where $\langle t_{\rm TP}^2\rangle = K^{(2)}(x_{B/A}|x_{A/B})/\phi_{B/A}(x_{A/B})$. Moreover, $\langle t_{\rm TP}\rangle$ stands for $\tau^{\rm TP}(x_B|x_A)$ or $\tau^{\rm TP}(x_A|x_B)$. In order to obtain $\langle t_{\rm TP}^2\rangle$ we need to first obtain the second moment $K^{(2)}(x_{B/A}|x_0)$ of the FPTD. Similar to $K^{(1)}(x_{B/A}|x_0,\pm1)$, the expression $K^{(2)}(x_{B/A}|x_0,\pm1)$ obey the backward equations

$$\begin{aligned}-2K^{(1)}(x_{A/B}|x_0,+1)&=(f(x_0)+v)\frac{\partial}{\partial x_0}K^{(2)}(x_{A/B}|x_0,+1)+\gamma\big[K^{(2)}(x_{A/B}|x_0,-1)-K^{(2)}(x_{A/B}|x_0,+1)\big],\\ -2K^{(1)}(x_{A/B}|x_0,-1)&=(f(x_0)-v)\frac{\partial}{\partial x_0}K^{(2)}(x_{A/B}|x_0,-1)+\gamma\big[K^{(2)}(x_{A/B}|x_0,+1)-K^{(2)}(x_{A/B}|x_0,-1)\big].\end{aligned} \tag{23}$$

Here, we present the forms of $K^{(2)}(x_B|x_0,\pm1)$. A derivation of $K^{(2)}(x_A|x_0,\pm1)$ is shown in App. C.

Defining

$$\begin{aligned}\omega_B(x_0) &= K^{(2)}(x_B|x_0,+1)+K^{(2)}(x_B|x_0,-1),\\ \theta_B(x_0) &= K^{(2)}(x_B|x_0,+1)-K^{(2)}(x_B|x_0,-1),\end{aligned} \tag{24}$$

Eq. (23) can be rewritten as

$$\begin{aligned}f(x_0)\frac{\partial}{\partial x_0}\omega_B(x_0)+v\frac{\partial}{\partial x_0}\theta_B(x_0) &= -2K^{(1)}(x_B|x_0,+1)-2K^{(1)}(x_B|x_0,-1),\\ f(x_0)\frac{\partial}{\partial x_0}\theta_B(x_0)+v\frac{\partial}{\partial x_0}\omega_B(x_0) &= 2\gamma\theta_B(x_0)+2\big[K^{(1)}(x_B|x_0,-1)-K^{(1)}(x_B|x_0,+1)\big].\end{aligned} \tag{25}$$

With to the boundary conditions (6) we obtain

$$\begin{aligned}\theta_B(x_0) &= \frac{2}{M_1(x_0)}\int_{x_A}^{x_0}\frac{M_1(x)K^{(1)}(x_B|x,-1)}{f(x)-v}dx-\frac{2}{M_1(x_0)}\int_{x_A}^{x_0}\frac{M_1(x)K^{(1)}(x_B|x,+1)}{f(x)+v}dx+\frac{D_3}{M_1(x_0)},\\ \omega_B(x_0) &= -2\int_{x_A}^{x_0}\frac{K^{(1)}(x_B|x,-1)}{f(x)-v}dx-4\gamma v\int_{x_A}^{x_0}\int_{x_A}^{x}\frac{M_1(y)K^{(1)}(x_B|y,-1)}{f(y)-v}dy\frac{dx}{M_1(x)(f^2(x)-v^2)}\\ &\quad -4\gamma v\int_{x_A}^{x_0}\frac{K^{(1)}(x_B|x,+1)}{f(x)+v}dx+2\int_{x_A}^{x_0}\int_{x_A}^{x}\frac{M_1(y)K^{(1)}(x_B|y,+1)}{f(y)+v}dy\frac{dx}{M_1(x)(f^2(x)-v^2)}\\ &\quad -2\gamma v D_3\int_{x_A}^{x_0}\frac{dx}{M_1(x)(f^2(x)-v^2)}+D_4,\end{aligned} \tag{26}$$

where $D_4 = D_3/[M_1(x_A)]$, and D_3 can be derived from $\theta_B(x_B)+\omega_B(x_B)=0$. $M_1(x_0)$ appears in Eq. (18) and $K^{(2)}(x_{B/A}|x_0) = \frac{1}{2}[K^{(2)}(x_{B/A}|x_0,+1)+K^{(2)}(x_{B/A}|x_0,-1)]$. Then we can determine the theoretical results of C_V from Eq. (22).

C. Mean transition path shape

We define $\tau^{\rm TP}_{\rm shape}(x_0|x_A)$ and $\tau^{\rm TP}_{\rm shape}(x_0|x_B)$ as the mean transition path shapes of RTPs from x_A/x_B to x_0, respectively. They are given by [49]

$$\begin{aligned}\tau^{\rm TP}_{\rm shape}(x_0|x_A) &= \tau^{\rm TP}(x_B|x_A)-\tau^{\rm TP}(x_B|x_0),\\ \tau^{\rm TP}_{\rm shape}(x_0|x_B) &= \tau^{\rm TP}(x_A|x_B)-\tau^{\rm TP}(x_A|x_0).\end{aligned} \tag{27}$$

The analytical results of the transition path shape for RTPs are given in App. C, i.e. Eqs. (C3-C6).

D. Distribution of unproductive attempts

As shown in Fig. 1, showing simulations results of Eq. (1), we observe from the sample trajectories (gray lines) of RTPs the unproductive fluctuations in the forward and reverse directions, shown by the red and pink lines, respectively. The yellow lines represent transition paths in the transition path region $[-1,3]$.

$p(x|{\rm NPF}_F)$ and $p(x|{\rm NPF}_R)$ are distributions of forward and reverse unproductive attempts, respectively. The position distribution for forward or reverse unsuccessful reaction attempts can be expressed, respectively, as [59]

$$\begin{aligned}p(x|{\rm NPF}_F) &\propto [\phi_A(x)]^2 p_{\rm eq}(x),\\ p(x|{\rm NPF}_R) &\propto [\phi_B(x)]^2 p_{\rm eq}(x),\end{aligned} \tag{28}$$

where $p_{\rm eq}(x)$ is the stationary distribution of the system (1). $p_{\rm eq}(x)$ can be obtained from Eq. (2) [38], yielding

$$p_{\rm eq}(x) \propto \frac{1}{v^2-f^2(x)}\exp\left[2\gamma\int_0^x\frac{f(y)}{v^2-f^2(y)}dy\right]. \tag{29}$$

For the linear potential case, in Eq. (29), $p_{\rm eq}(x)\propto\frac{1}{v^2-b^2}\exp\left(\frac{2\gamma b}{v^2-b^2}x\right)$.

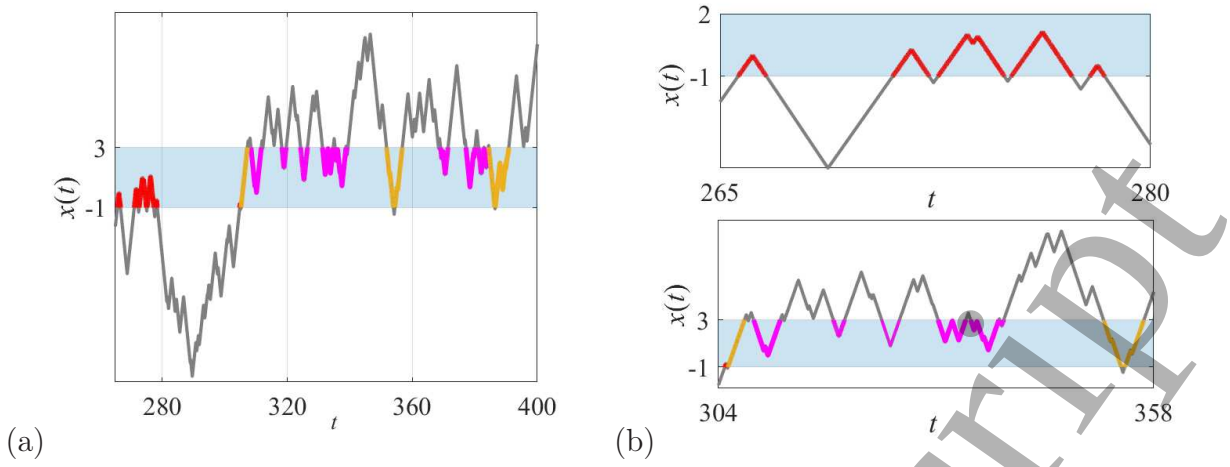

FIG. 1: (a) Sketch of the RTP trajectory of Eq. (1) including the transition paths and unproductive attempts. The transition region is $[x_A, x_B] = [-1, 3]$. (b) Unproductive attempts. Red lines are unproductive attempts from x_A to x_A, pink lines are unproductive attempts from x_B to x_B, and yellow lines stand for transition paths.

E. Mean duration of unproductive fluctuations

The mean duration of unproductive fluctuations, i.e., the mean return times $\tau_R(x_A \to x_A)$ and $\tau_R(x_B \to x_B)$. These are also the forward and reverse durations of unproductive fluctuations, respectively. Then, $\tau_R(x_A \to x_A)$ and $\tau_R(x_B \to x_B)$ satisfy [59]

$$\begin{aligned} \tau_R(x_A \to x_A) &= \frac{K^{(1)}(x_A|x_A)}{\phi_A(x_A)}, \\ \tau_R(x_B \to x_B) &= \frac{K^{(1)}(x_B|x_B)}{\phi_B(x_B)}, \end{aligned} \tag{30}$$

where $K^{(1)}(x_A|x_A)$ and $K^{(1)}(x_B|x_B)$ can be obtained from Eq. (D1).

III. RESULTS

We proceed with the analysis of how the systems parameters, such as the height of the potential barrier, on the transition path properties of RTPs, we work with the linear potential function $V(x) = Ux/2$ as an example, other potential functions can be studied analogously. Here, we assume that $|U| < 2v$, otherwise the RTP always just moves in one direction, which would result in a rather trivial transition path behaviour.

A. Splitting probability

The variation of the splitting probability $\phi_A(x_0)$ with the initial position x_0 is shown in Fig. 2. As expected, $\phi_A(x_0)$ decreases as x_0 increases. However, as can be seen from Eq. (B10), the decrease with x_0 is not linear, which is significantly different from the free RTP case [70]. The splitting probability of the particle initially in the $+1$ state is significantly smaller than that of the -1 state, i.e., $\phi_A^{+1}(x_0, +1)$ is less than $\phi_A^{+1}(x_0, -1)$, and $\phi_A^{-1}(x_0, +1)$ is less than $\phi_A^{-1}(x_0, -1)$. Moreover, the splitting probability is the same when the particles have the same initial position x_0 and the same σ_j state. Thus, as the particle gets closer to $x_A = -1$, it has a higher chance to escape through the left-hand boundary x_A.

Fig. 3 compares the analytical splitting probability $\phi_B(x_0)$ (solid lines), for different cases, with simulation results of the Langevin equation (1) (symbols). Unlike the splitting probability $\phi_A(x_0)$, $\phi_B(x_0)$ gradually increases with growing x_0, but again the relationship is non-linear. We see that $\phi_B^{\pm 1}(x_0, +1)$ is greater than $\phi_B^{\pm 1}(x_0, -1)$. Moreover, $\phi_B^{-1}(x_0, \pm 1)$ and $\phi_B^{+}(x_0, \pm 1)$ are the same. Here, the probability for the particle to exit at the left-hand boundary $x_A = -1$ is always equal to the case at the right-hand boundary x_B. Indeed, Figs. 2 and 3 demonstrate that the

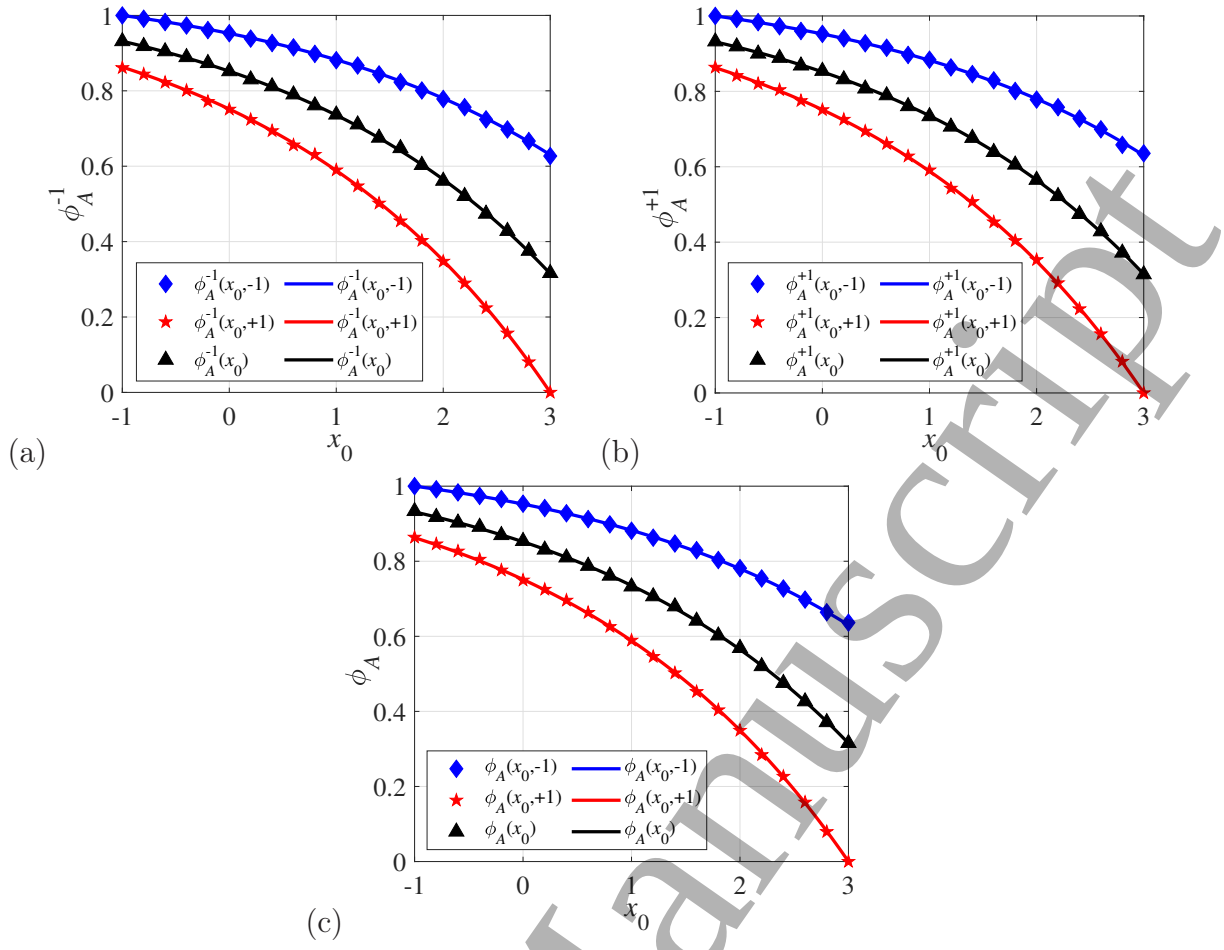

FIG. 2: Splitting probability of an RTP as a function of x_0, with the parameters $V(x) = Ux/2$, $U = -4$, $\gamma = 2.0$, and $v = 5.0$. The transition region is $[-1, 3]$. We find excellent agreement between the numerical simulations (symbols) and the theoretical predictions (lines) from Eqs. (B9) and (B10).

analytic results of the splitting probabilities, shown by the solid lines, is very good quantitative agreement with the numerical results from Monte Carlo simulations.

B. Transition path time and COV

We now consider the forward and reverse transition path times $\tau(x_B|x_A)$ and $\tau(x_A|x_B)$, as well as the COV C_V of the transition path time distribution. We specifically consider effects of the particle speed v, tumble rate γ, transition region boundaries x_A and x_B, and the steepness U of the potential function U on $\tau(x_B|x_A)$ and $\tau(x_A|x_B)$, as shown in Figs. 4 and 5, respectively.

We see that upon increasing v the γ-dependence of $\tau(x_B|x_A)$ approaches a linear dependence, see panel (a) in Fig. 4. From panel (b), as intuitively expected, larger v leads to smaller $\tau(x_B|x_A)$. Changing the size of the transition path region, panel (c) demonstrates that $\tau(x_B|x_A)$ monotonically decreases with $x_B - x_A$. In panel (d), $\tau(x_B|x_A)$ is shown to increase as $x_B - x_A$ increases. To obtain additional insight into the behaviour of the RTPs in an external potential we plot in panels (e) and (f) the values of $\tau(x_B|x_A)$ as function of U. We observe that $\tau(x_B|x_A)$ is monotonically increasing with U. We note that for the largest γ value a plateau-like region emerges around $U = 0$. As evidenced in this figure, the theoretical solutions for $\tau(x_B|x_A)$ are nicely consistent with Monte Carlo simulations of the Langevin equation (1).

Similarly, in Fig. 5, the effects of the systems parameters on the reverse transition path time $\tau(x_A|x_B)$ are considered. $\tau(x_A|x_B)$ exhibits a monotonic behaviour with respect to these parameters. In panels (a-d) we present the variation of $\tau(x_A|x_B)$ with γ, v, and $x_B - x_A$, demonstrating consistency with that of $\tau(x_B|x_A)$. As seen in panels (e) and (f), the difference to the case in Fig. 4 is that growing U effects a decrease in $\tau(x_A|x_B)$. Again, as in panel (e) of Fig. 4,

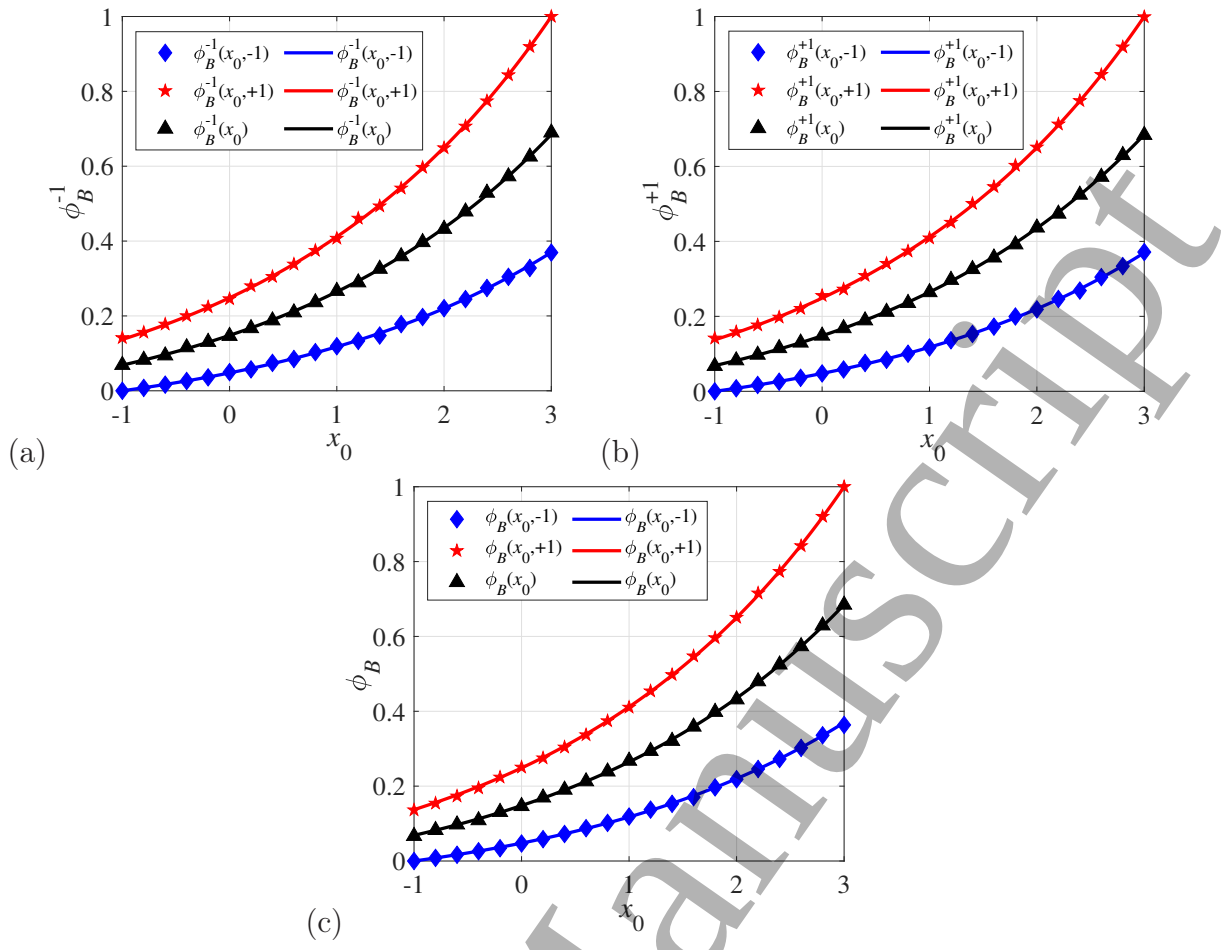

FIG. 3: Splitting probability of an RTP as a function of x_0, where the parameters are $V(x) = Ux/2$, $U = -4$, $\gamma = 2.0$, and $v = 5.0$. The transition region is $[-1, 3]$. The lines are analytic results from Eqs. (B9) and (B10), the symbols represent numerical results. The agreement with the theoretical predictions is excellent.

panel (e) exhibits a plateau-like crossover around vanishing U. Generally, excellent agreement between the theoretical results and the numerical simulations is observed.

To further detail the difference between the situations of Figs. 4 and 5, we plot in Fig. 6 the dependence of the difference $\tau(x_B|x_A) - \tau(x_A|x_B)$ on the systems parameters. The difference $\tau(x_B|x_A) - \tau(x_A|x_B)$ the the transition path times is shown as function of γ and v in panels (a) and (b), respectively. Remarkably, the difference $\tau(x_B|x_A) - \tau(x_A|x_B)$ is completely independent of γ, which is different from the free RTP case [70]. In fact, we previously proved theoretically that the system parameters cannot effect a symmetry breaking in the transition path properties of these RTPs for unconstrained motion (i.e., $\tau(x_B|x_A) = \tau(x_A|x_B)$) [70]. Panel (b) demonstrates that $\tau(x_B|x_A) - \tau(x_A|x_B)$ decreases with growing v, as intuitively expected. Panels (c) and (d) show the effect of the transition path region on the difference $\tau(x_B|x_A) - \tau(x_A|x_B)$, for various v and γ. In both cases a linear dependence is observed. As v increases, panel (c), the slope of decreases, i.e., $\tau(x_B|x_A))$ and $\tau(x_A|x_B)$ approach each other. In panel (d) we see that the different choices of γ do not affect the difference $\tau(x_B|x_A) - \tau(x_A|x_B)$. Finally, panels (e) and (f) show the dependence on the slope U of the external potential, for different γ and v. In both cases the difference of the transition path times. As shown by the dashed lines, the absolute values of the time difference are fully symmetric around $U = 0$, as they should. Summarising Fig. 6, the time difference $\tau(x_B|x_A) - \tau(x_A|x_B)$ decreases monotonically with the particle speed v, left-hand boundary x_A, and the steepness U.

From Figs. 4 to 6 we see that the forward and reverse transition path times differ significantly. In fact, this can be rationalised as follows. The potential function defined used here is $V(x) = Ux/2$. When $U > 0$, in the forward direction, the particle moves from x_A to x_B, and the RTP is in the process of climbing the potential. In the reverse direction, the particle moves from x_B to x_A, and the RTP is going downhill. When for this situation $U > 0$ the value of U increases, the reverse transition path time becomes significantly less than the forward transition path time. The difference between $\tau(x_A|x_B)$ and $\tau(x_B|x_A)$ thus increases as the absolute value of U increases. (When $U < 0$, the

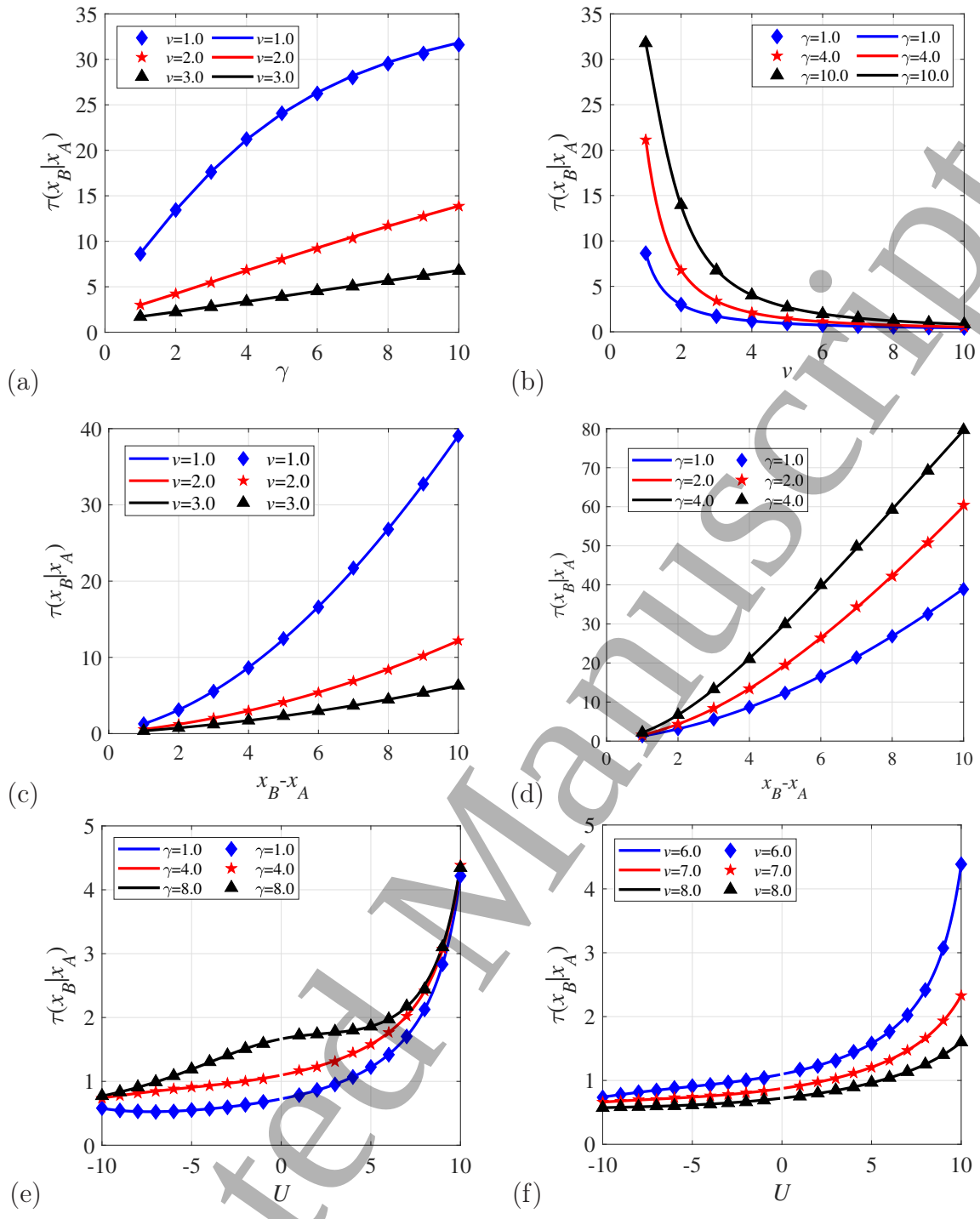

FIG. 4: Forward transition path times $\tau(x_B|x_A)$. (a) $\tau(x_B|x_A)$ as function of γ for different values of v with $U = 0.2$, $x_A = -1$, and $x_B = 3$. (b) $\tau(x_B|x_A)$ versus v for different values of γ with $U = 0.2$, $x_A = -1$, and $x_B = 3$. (c) $\tau(x_B|x_A)$ as function of $x_B - x_A$ for various v with $U = 0.2$, $\gamma = 1.0$, and $x_A = 2$. (d) $\tau(x_B|x_A)$ as function of $x_B - x_A$ for various γ with $U = 0.2$, $v = 1.0$, and $x_B = 0$. (e) $\tau(x_B|x_A)$ versus U for various γ with $v = 6.0$, $x_A = -1.0$, and $x_B = 3.0$. (f) $\tau(x_B|x_A)$ as function of U for various v with $\gamma = 4.0$, $x_A = -1.0$, and $x_B = 3.0$. Solid lines correspond to the predictions from Eq. (C5), while the symbols represent numerical simulations of Eq. (1). Both show excellent agreement.

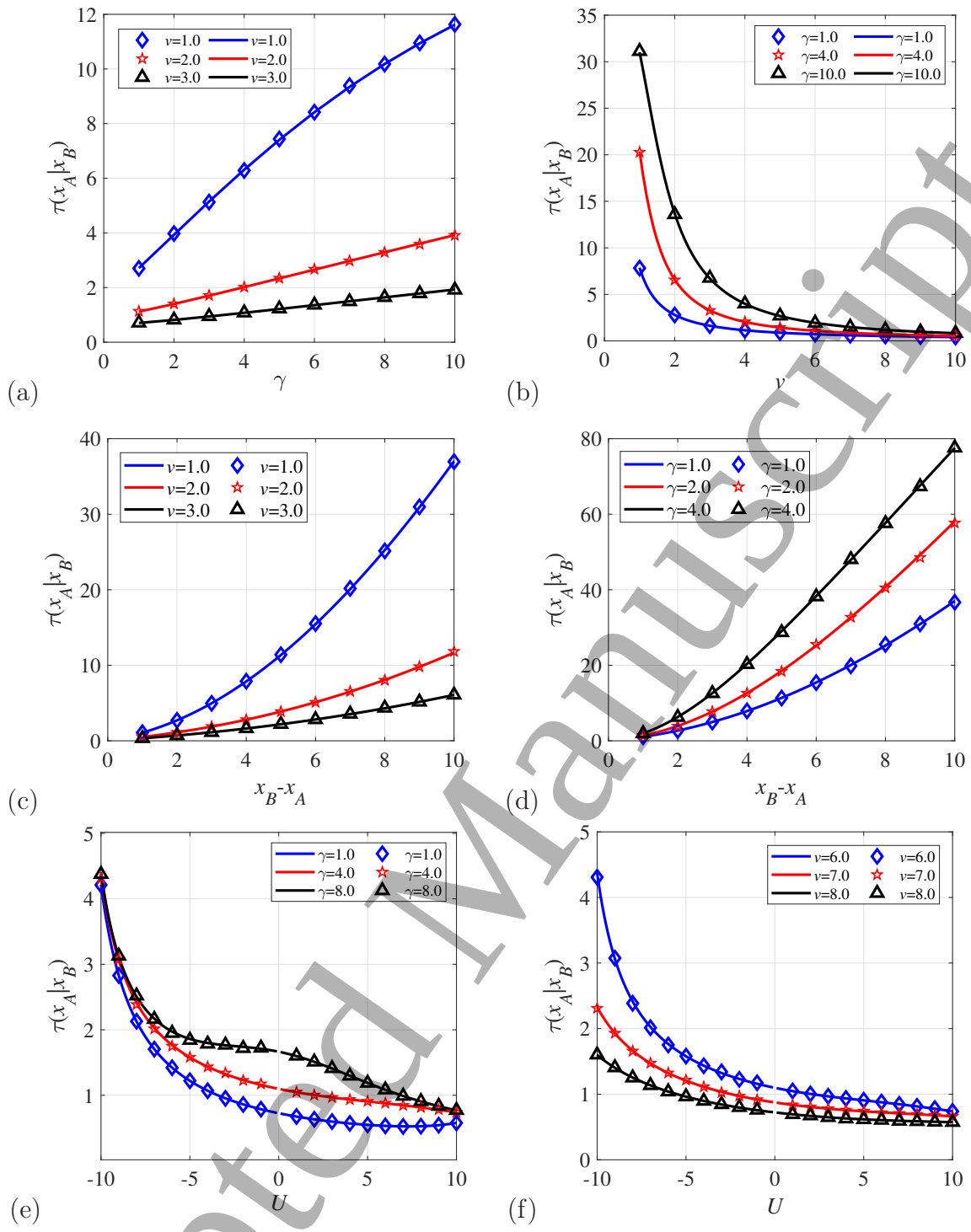

FIG. 5: Reverse transition path times $\tau(x_A|x_B)$. (a) $\tau(x_A|x_B)$ as a function of γ for different values of v with $U = 0.2$, $x_A = -1$, and $x_B = 3$. (b) Plot of $\tau(x_A|x_B)$ vs v for different values of γ with $U = 0.2$, $x_A = -1$, and $x_B = 3$. (c) $\tau(x_A|x_B)$ as function of $x_B - x_A$ for various v with $U = 0.2$, $\gamma = 1.0$, and $x_A = 2$. (d) $\tau(x_A|x_B)$ versus $x_B - x_A$ for various γ with $U = 0.2$, $v = 1.0$, and $x_B = 0$. (e) $\tau(x_A|x_B)$ as function of U for various γ with $v = 6.0$, $x_A = -1.0$, and $x_B = 3.0$. (f) $\tau(x_A|x_B)$ as function of U for various v with $\gamma = 4.0$, $x_A = -1.0$, and $x_B = 3.0$. Solid lines represent Eq. (C5), the symbols represent the numerical simulations from Monte Carlo simulations.

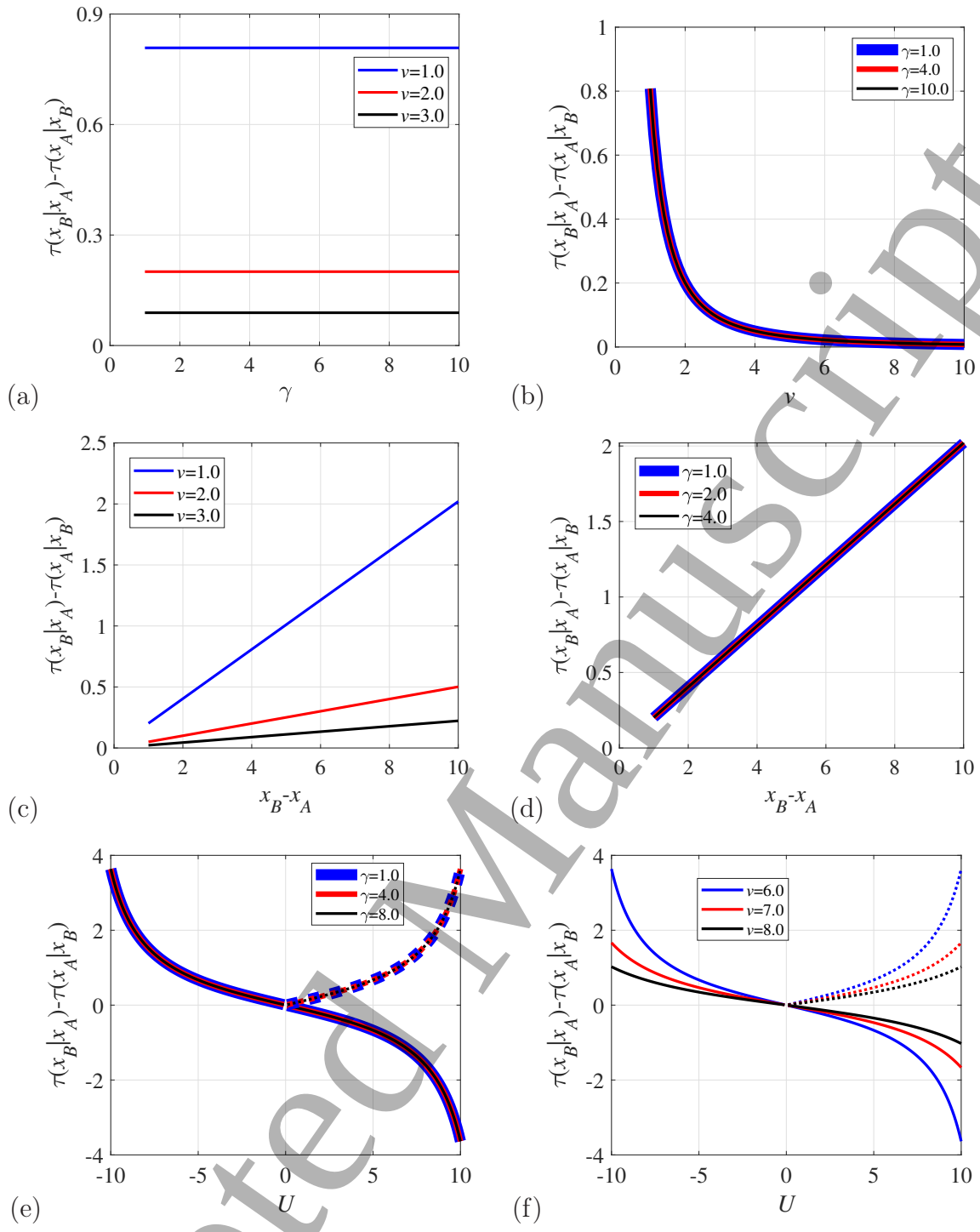

FIG. 6: Difference of the transition path times in both directions from Eq. (C5). (a) $\tau(x_B|x_A) - \tau(x_A|x_B)$ as a function of γ for different values of v with $U = 0.2$, $x_A = -1$, and $x_B = 3$. (b) $\tau(x_B|x_A) - \tau(x_A|x_B)$ versus v for different values of γ with $U = 0.2$, $x_A = -1$, and $x_B = 3$. (c) $\tau(x_B|x_A) - \tau(x_A|x_B)$ as function of $x_B - x_A$ for various v with $U = 0.2$, $\gamma = 1.0$, and $x_A = 2$. (d) $\tau(x_B|x_A) - \tau(x_A|x_B)$ versus $x_B - x_A$ for various γ with $U = 0.2$, $v = 1.0$, and $x_B = 0$. (e) $\tau(x_B|x_A) - \tau(x_A|x_B)$ as function of U for various γ with $v = 6.0$, $x_A = -1.0$, and $x_B = 3.0$. (f) $\tau(x_B|x_A) - \tau(x_A|x_B)$ versus U for various v with $\gamma = 4.0$, $x_A = -1.0$, and $x_B = 3.0$. Solid lines represent the theoretical predictions of $\tau(x_B|x_A) - \tau(x_A|x_B)$, the dotted lines are the absolute values of the theoretical predictions of $\tau(x_B|x_A) - \tau(x_A|x_B)$ for $U > 0$.

situation is opposite.) This is exactly the result presented in Figs. 6(e) and (f).

In order to consider the influence of the system parameters on the COV C_V, we choose C_V for the forward transition path time distribution as an example to carry out a specific discussion. Fig. 7 displays the C_V as function of the systems parameters. As can be seen from panels (a) to (d), when U is positive, $C_V < 1$ for all selected parameters. Interestingly, one observes a clear non-monotonic behaviour as function of γ, panel (a). Overall, the dependence of C_V on the parameters exhibits quite diverse behaviour. When looking at the influence of U on C_V, it gradually decreases with growing U. For very negative values of U, C_V exceeds unity, i.e., leading to wider than exponential distributions of the transition path times.

The COV C_V for additional parameter values is shown in Fig. 8, concentrating on negative values of U. The variation of C_V with γ and v in panels (a) and (b) is consistent with those shown in the same panels of Fig. 7. In particular, panel (a) demonstrates again a clear maximum of C_V as function of γ. For the selected parameters, smaller v or U values allow C_V to exceed unity. As shown in panels (c) and (d), depending on the choice of the parameters the functional dependence of C_V on x_A or x_B switches between monotonic behaviour and a slight maximum.

C. Mean transition path shape

We continue by discussing the effect of the systems parameters on the mean transition path shapes $\tau^{\rm TP}_{\rm shape}(x_0|x_A)$ and $\tau^{\rm TP}_{\rm shape}(x_0|x_B)$, which are obtained from simulations of Eq. (1) and compared with those obtained analytically in Eq. (27).

In Fig. 9 shows the variation with the initial position x_0 of the transition path shapes. Panels (a), (c), and (e) show the case $U > 0$; panels (b), (d), and (f) represent the case $U < 0$. As shown in (a) and (b), the transition path shapes show the expected monotonous dependence on x_0. Moreover, a monotonous dependence on v is seen: An increase of v effects a decrease of $\tau^{\rm TP}_{\rm shape}(x_0|x_A)$ and $\tau^{\rm TP}_{\rm shape}(x_0|x_B)$ for fixed x_0. Panels (c) and (d) show that for larger γ effects higher transition path shape amplitudes. However, the influence of U on $\tau^{\rm TP}_{\rm shape}(x_0|x_A)$ and $\tau^{\rm TP}_{\rm shape}(x_0|x_B)$ is more subtle. Panels (e) and (f) demonstrate that regardless of the (positive or negative) value of U, $\tau^{\rm TP}_{\rm shape}(x_0|x_B)$ decreases with the increase of U, while $\tau^{\rm TP}_{\rm shape}(x_0|x_A)$ shows the opposite dependence. For negative values of U, in panels (b), (d), and (f), we see that $\tau^{\rm TP}_{\rm shape}(x_0|x_B)$ is larger than $\tau^{\rm TP}_{\rm shape}(x_0|x_A)$.

We note that the results shown in Fig. 9 demonstrate that the quantities $\tau^{\rm TP}_{\rm shape}(x_0|x_A)$ and $\tau^{\rm TP}_{\rm shape}(x_0|x_B)$ are no longer symmetric for the chosen systems parameter, i.e., the potential causes a visible asymmetry of the transition path shape. This asymmetry becomes more pronounced as the absolute value of U increases, see panels (e) and (f). Especially when the $U > 0$, the values of $\tau^{\rm TP}_{\rm shape}(x_0|x_A)$ are larger than those of $\tau^{\rm TP}_{\rm shape}(x_0|x_B)$. The trend is reversed for the case $U < 0$.

D. Position distribution of unproductive attempts

We now consider the positional distribution $p(x|{\rm NPF}_F)$ and $p(x|{\rm NPF}_R)$ for unproductive attempts in forward and reverse directions, respectively. According to Eqs. (28) and (B10), the monotonic behaviour of $p(x|{\rm NPF}_F)$ and $p(x|{\rm NPF}_R)$ is clearly visible. As shown in Fig. 10, the forward distribution $p(x|{\rm NPF}_F)$ is a decreasing function of the position x for fixed system parameters. For symmetry reasons, the dependence on x is increasing for $p(x|{\rm NPF}_R)$, as seen in Fig. 11.

Panels (a) and (b) in Fig. 10 show that when the particles are close to the left boundary x_A of the transition path region, they have a high probability $p(x|{\rm NPF}_F)$ for unproductive attempts. Indeed, it can be shown from Eqs. (28) and (B10) that $p(x|{\rm NPF}_F)$ has a maximum at x_A. Simultaneously, the distribution of unproductive paths decreases as v increases. However, it increases with growing γ. As shown in panels (c) and (d), a larger U leads to an increase of $p(x|{\rm NPF}_F)$.

Fig. 11 shows the opposite case of the reverse direction, i.e., $p(x|{\rm NPF}_R)$, for different values of v, γ and U. We see that here the maximum is attained at the right boundary, x_B. The influences of v, γ, and U on $p(x|{\rm NPF}_R)$ show an opposite trend to the behaviour in Fig. 10.

E. Mean duration of unproductive fluctuations

Fig. 12, shows the mean durations $\tau(x_A|x_A)$ and $\tau(x_B|x_B)$ as function of the systems parameters of the duration of the forward and reverse unsuccessful path. Panels (a) and (c) show plots of $\tau(x_A|x_A)$ as function of v or γ for different values of U, as calculated from Eq. (D1). Increasing v and γ lead to a decrease of $\tau(x_A|x_A)$ at larger values,

with an initial increase. Similarly, panels (b) and (d) show a decreasing trend of $\tau(x_B|x_B)$ for larger values of v or γ. A quite rich behaviour is shown by the mean durations $\tau(x_A|x_A)$ and $\tau(x_B|x_B)$ in dependence of U on variation of γ and v. In panels (e) and (f) we see that with increase of U, $\tau(x_A|x_A)$ increases initially, then turning into a decreasing trend. Moreover, $\tau(x_B|x_B)$ and $\tau(x_A|x_A)$ are symmetric with respect to $U = 0$.

From the results presented in Figs. 4, 5, and 12, we see that as the tumbling rate γ increases, the forward and reverse transition path times $\tau(x_B|x_A)$ and $\tau(x_A|x_B)$ both increase, while the durations of the unsuccessful forward and reverse paths $\tau(x_A|x_A)$ and $\tau(x_B|x_B)$ decrease. In fact, according to the motion characteristics of an RTP, the particles are affected by the tumbling rate during their motion. Thus, when the particles approachies the target and the motion direction of the particles suddenly changes, the particle moves backward and thus away from the target position. Therefore, the random tumbling characteristic of the RTP may hinder the escape behavior of the particles and promote unsuccessful paths.

IV. CONCLUSIONS

We here provided an efficient theoretical scheme to analyse the transition path properties for an RTP under the influence of an external potential. Specifically, we studied the effect of the particle velocity, the tumble rate, the potential stiffness, and the transition path region on the transition path properties for a one-dimensional RTP. In addition, we also determined the theoretical description of the failed (unproductive) attempts for RTPs. The nonequilibrium behaviour of such RTPs results in transition path properties that are significantly different from those of equilibrium systems. Particularly, the transition path properties exhibit an interesting monotonous dependence on the system parameters. All our theoretical results are confirmed by Monte Carlo simulations.

When an external potential is introduced, we find that the tumble rate of the RTP has no effect on the time difference of the transition path times in the two directions. Interestingly, our theoretical results demonstrate that the symmetry properties of the transition path time and shape are quite sensitive to the steepness of the potential: increasing stiffness leads to more pronounced asymmetry. Moreover, the presence of the potential accelerates the escape of the RTP. These results will be useful in the study of bacterial chemotaxis in complex systems, their community behaviour, or phenomena such as the transport of nanoparticles in fluids. The research on the unsuccessful paths of RTPs is expected to promote the related work in life, medicine and other fields, and for the investigation of active drug delivery.

Our method succeeds in obtaining theoretical results of transition path properties of RTPs subjected to an external potential. These were shown to be in excellent agreement with Monte Carlo simulations results. In agreement with the results of Ref. [71], where the phenomenon of symmetry breaking in the transition path time during a telegraph process was observed in the presence of an external potential function, we indeed found a pronounced asymmetry in the settings of our system. It will be interesting to set up our system for telegraphic noise. Moreover, the analysis presented here may also be generalised to other active systems, such as active Brownian particles.

Acknowledgments

The authors express their gratitude to the editors and the reviewers for the helpful comments. Y. Xu was partially supported by the Key International (Regional) Joint Research Program of the National Science Foundation of China (No. 12120101002). H. Li thanks the National Natural Science Foundation of China (12202145). Z.Q. Wang thanks the National Natural Science Foundation of China (12202332). R.M. acknowledges the German Science Foundation (DFG, grant no. ME 1535/12-1) for support.

Appendix A: Detailed derivation of Eq. (5)

Here, we focus on the derivation of $K(x_B, t|x_0, \sigma_j)$, the case $K(x_A, t|x_0, \sigma_j)$ can be obtained in a similar manner.

Following Eq. (1), we derive the backward master equation for $K(x_B, t|x_0, +1)$ and $K(x_A, t|x_0, -1)$. To this end we first write the disretised version of Eq. (1). We suppose that at time t, the RTP is in the state $\sigma(t) = +1$. Then, one obtains [72]

$$x(t+dt) = \begin{cases} x(t), & \text{with probability } \gamma dt \text{ and } \sigma(t+dt) = -1 \\ x(t) + [f(x) + v]dt, & \text{with probability } 1 - \gamma dt \text{ and } \sigma(t+dt) = +1. \end{cases} \tag{A1}$$

Conversely, when the RTP particle is in the state $\sigma(t) = -1$ at time t, we find

$$x(t+dt) = \begin{cases} x(t), & \text{with probability } \gamma dt \text{ and } \sigma(t+dt) = +1 \\ x(t) + [f(x) - v]dt, & \text{with probability } 1 - \gamma dt \text{ and } \sigma(t+dt) = -1. \end{cases} \tag{A2}$$

Now we assume that the RTP starts to move at time $t = 0$ at the initial position $x(0) = x_0$. At first, there is no change of state such that $\sigma(t) = +1$ with probability $1 - \gamma dt$. According to Eq. (1), from time $t = 0$ to time $t = dt$, the RTP has the velocity $\frac{dx(t)}{dt} = f(x) + v$, therefore, the RTP's position is $x_0 + [f(x) + v]dt$ at time dt. In addition, if the RTP particle tumbles and the state changes to $\sigma(t) = -1$, it has position $x_0 + [f(x) - v]dt$ with probability γdt. Then, we arrive at

$$\begin{aligned} K(x_B, t+dt|x_0, +1) =& (1 - \gamma dt)K(x_B, t|x_0 + [f(x_0) + v]dt, +1) \\ &+ \gamma dt K(x_B, t|x_0 + [f(x_0) - v]dt, -1). \end{aligned} \tag{A3}$$

In order to solve Eq. (A3), we perform the Taylor expansion of the first and second terms to first order in dt, resulting in

$$\begin{aligned} K(x_B, t|x_0 + [f(x_0) + v]dt, +1) &= K(x_B, t|x_0, +1) + [f(x_0) + v]dt\partial_{x_0} K(x_B, t|x_0, +1), \\ K(x_B, t|x_0 + [f(x_0) - v]dt, -1) &= K(x_B, t|x_0, -1) + [f(x_0) - v]dt\partial_{x_0} K(x_B, t|x_0, -1). \end{aligned} \tag{A4}$$

Substituting Eq. (A4) into Eq. (A3) and retainiing only first-order terms of order dt, we find

$$\begin{aligned} K(x_B, t+dt|x_0, +1) =& K(x_B, t|x_0, +1) + [f(x_0) + v]dt\partial_{x_0} K(x_B, t|x_0, +1) \\ &+ \gamma dt[K(x_B, t|x_0, -1) - K(x_B, t|x_0, +1)]. \end{aligned} \tag{A5}$$

Then, taking the limit $dt \to 0$ leads to

$$\partial_t K(x_B, t|x_0, +1) = [f(x_0) + v]\partial_{x_0} K(x_B, t|x_0, +1) + \gamma[K(x_B, t|x_0, -1) - K(x_B, t|x_0, +1)]. \tag{A6}$$

$K(x_A|x_0, \sigma_j)$ can be obtained in a similar manner. Finally, according to Eq. (3), we obtain from Eq. (A6) the set of equations

$$\begin{aligned} -nK^{(n-1)}(x_{A/B}|x_0, +1) &= (f(x_0) + v)\frac{\partial}{\partial x_0} K^{(n)}(x_{A/B}|x_0, +1) + \gamma\left[K^{(n)}(x_{A/B}|x_0, -1) - K^{(n)}(x_{A/B}|x_0, +1)\right], \\ -nK^{(n-1)}(x_{A/B}|x_0, -1) &= (f(x_0) - v)\frac{\partial}{\partial x_0} K^{(n)}(x_{A/B}|x_0, -1) + \gamma\left[K^{(n)}(x_{A/B}|x_0, +1) - K^{(n)}(x_{A/B}|x_0, -1)\right]. \end{aligned} \tag{A7}$$

Appendix B: Detailed theoretical results for the splitting probability $\phi_B(x_0)$

The splitting probabilities $\phi_B^{\sigma_j}(x_0, \pm 1)$ satisfy

$$\begin{aligned} (f(x_0) + v)\frac{\partial}{\partial x_0}\phi_B^{\sigma_j}(x_0, +1) + \gamma\left[\phi_B^{\sigma_j}(x_0, -1) - \phi_B^{\sigma_j}(x_0, +1)\right] = 0, \\ (f(x_0) - v)\frac{\partial}{\partial x_0}\phi_B^{\sigma_j}(x_0, -1) + \gamma\left[\phi_B^{\sigma_j}(x_0, +1) - \phi_B^{\sigma_j}(x_0, -1)\right] = 0. \end{aligned} \tag{B1}$$

We define $\rho_B(x_0) = \phi_B^{-1}(x_0, +1) + \phi_B^{-1}(x_0, -1)$ and $\mu_B(x_0) = \phi_B^{-1}(x_0, -1) - \phi_B^{-1}(x_0, +1)$. Therefore, Eq. (B1) can be rewritten as

$$\begin{aligned} f(x_0)\frac{\partial}{\partial x_0}\rho_B(x_0) + v\frac{\partial}{\partial x_0}\mu_B(x_0) = 0, \\ f(x_0)\frac{\partial}{\partial x_0}\mu_B(x_0) + v\frac{\partial}{\partial x_0}\rho_B(x_0) - 2\gamma\mu_B(x_0) = 0. \end{aligned} \tag{B2}$$

Then, we obtain $\phi_B^{-1}(x_0,\pm 1)$,

$$\begin{aligned}\phi_B^{-1}(x_0,-1) &= C_5\int_{x_0}^{x_B}\frac{\gamma v}{f^2(x)-v^2}N_1(x)dx+\frac{C_2}{2}+\frac{C_5}{2}N_1(x_0),\\ \phi_B^{-1}(x_0,+1) &= C_5\int_{x_0}^{x_B}\frac{\gamma v}{f^2(x)-v^2}N_1(x)dx+\frac{C_6}{2}-\frac{C_5}{2}N_1(x_0),\end{aligned} \tag{B3}$$

where $C_6=2-C_5$, $C_5=-1\big/\big[\int_{x_A}^{x_B}\frac{\gamma v}{f^2(x)-v^2}N_1(x)dx-\frac{1}{2}N_1(x_A)-\frac{1}{2}\big]$, and $N_1(x_0)$ appears under Eq. (10).

Similarly, we find

$$\begin{aligned}\phi_B^{+1}(x_0,-1) &= -C_7\int_{x_A}^{x_0}\frac{\gamma v}{f^2(x)-v^2}N_1(x)dx+\frac{C_8}{2}+\frac{C_7}{2}N_1(x_0),\\ \phi_B^{+1}(x_0,+1) &= C_7\int_{x_A}^{x_0}\frac{\gamma v}{f^2(x)-v^2}N_1(x)dx+\frac{C_8}{2}-\frac{C_7}{2}N_1(x_0),\end{aligned} \tag{B4}$$

where $C_8=C_7N_1(x_A)$, and $C_7=1\big/\left[-\int_{x_A}^{x_B}\frac{\gamma v}{f^2(x)-v^2}N_1(x)dx+\frac{1}{2}N_1(x_A)+\frac{1}{2}\right]$.

For the case of a linear potential, the force is $f(x)=b$ (i.e., $V(x)=Ux/2$, $b=-U/2$), and the results become

$$\begin{aligned}\phi_A^{+1}(x_0,-1) &= -\frac{vC_9}{2b}\left[\exp\left(\frac{2\gamma bx_0}{b^2-v^2}\right)-\exp\left(\frac{2\gamma bx_A}{b^2-v^2}\right)\right]+\frac{C_{10}}{2}-\frac{C_9}{2}\exp\left(\frac{2\gamma bx_0}{b^2-v^2}\right),\\ \phi_A^{+1}(x_0,+1) &= -\frac{vC_9}{2b}\left[\exp\left(\frac{2\gamma bx_0}{b^2-v^2}\right)-\exp\left(\frac{2\gamma bx_A}{b^2-v^2}\right)\right]+\frac{C_{10}}{2}+\frac{C_9}{2}\exp\left(\frac{2\gamma bx_0}{b^2-v^2}\right),\end{aligned} \tag{B5}$$

where $C_{10}=2+C_9\exp\left(\frac{2\gamma bx_A}{b^2-v^2}\right)$ and $C_9=-1\Big/\left[(\frac{1}{2}-\frac{v}{2b})\exp\left(\frac{2\gamma bx_B}{b^2-v^2}\right)+(\frac{1}{2}+\frac{v}{2b})\exp\left(\frac{2\gamma bx_A}{b^2-v^2}\right)\right]$. Similarly,

$$\begin{aligned}\phi_B^{+1}(x_0,-1) &= -\frac{vC_{11}}{2b}\left[\exp\left(\frac{2\gamma bx_0}{b^2-v^2}\right)-\exp\left(\frac{2\gamma bx_A}{b^2-v^2}\right)\right]+\frac{C_{12}}{2}-\frac{C_{11}}{2}\exp\left(\frac{2\gamma bx_0}{b^2-v^2}\right),\\ \phi_B^{+1}(x_0,+1) &= -\frac{vC_{11}}{2b}\left[\exp\left(\frac{2\gamma bx_0}{b^2-v^2}\right)-\exp\left(\frac{2\gamma bx_A}{b^2-v^2}\right)\right]+\frac{C_{12}}{2}+\frac{C_{11}}{2}\exp\left(\frac{2\gamma bx_0}{b^2-v^2}\right).\end{aligned} \tag{B6}$$

where $C_{12}=C_{11}\exp\left(\frac{2\gamma bx_A}{b^2-v^2}\right)$ and $C_{11}=1\Big/\left[(\frac{1}{2}-\frac{v}{2b})\exp\left(\frac{2\gamma bx_B}{b^2-v^2}\right)+(\frac{1}{2}+\frac{v}{2b})\exp\left(\frac{2\gamma bx_A}{b^2-v^2}\right)\right]$.

Moreover,

$$\begin{aligned}\phi_A^{-1}(x_0,-1) &= -\frac{vC_{13}}{2b}\left[\exp\left(\frac{2\gamma bx_0}{b^2-v^2}\right)-\exp\left(\frac{2\gamma bx_A}{b^2-v^2}\right)\right]+\frac{C_{14}}{2}-\frac{C_{13}}{2}\exp\left(\frac{2\gamma bx_0}{b^2-v^2}\right),\\ \phi_A^{-1}(x_0,+1) &= -\frac{vC_{13}}{2b}\left[\exp\left(\frac{2\gamma bx_0}{b^2-v^2}\right)-\exp\left(\frac{2\gamma bx_A}{b^2-v^2}\right)\right]+\frac{C_{14}}{2}+\frac{C_{13}}{2}\exp\left(\frac{2\gamma bx_0}{b^2-v^2}\right),\end{aligned} \tag{B7}$$

where $C_{14}=2+C_{13}\exp\left(\frac{2\gamma bx_A}{b^2-v^2}\right)$ and $C_{13}=-1\Big/\left[(\frac{1}{2}-\frac{v}{2b})\exp\left(\frac{2\gamma bx_B}{b^2-v^2}\right)+(\frac{1}{2}+\frac{v}{2b})\exp\left(\frac{2\gamma bx_A}{b^2-v^2}\right)\right]$, and

$$\begin{aligned}\phi_B^{-1}(x_0,-1) &= -\frac{vC_{15}}{2b}\left[\exp\left(\frac{2\gamma bx_0}{b^2-v^2}\right)-\exp\left(\frac{2\gamma bx_A}{b^2-v^2}\right)\right]+\frac{C_{16}}{2}-\frac{C_{15}}{2}\exp\left(\frac{2\gamma bx_0}{b^2-v^2}\right),\\ \phi_B^{-1}(x_0,+1) &= -\frac{vC_{15}}{2b}\left[\exp\left(\frac{2\gamma bx_0}{b^2-v^2}\right)-\exp\left(\frac{2\gamma bx_A}{b^2-v^2}\right)\right]+\frac{C_{16}}{2}+\frac{C_{15}}{2}\exp\left(\frac{2\gamma bx_0}{b^2-v^2}\right),\end{aligned} \tag{B8}$$

where $C_{16}=C_{15}\exp\left(\frac{2\gamma bx_A}{b^2-v^2}\right)$ and $C_{15}=1\Big/\left[(\frac{1}{2}-\frac{v}{2b})\exp\left(\frac{2\gamma bx_B}{b^2-v^2}\right)+(\frac{1}{2}+\frac{v}{2b})\exp\left(\frac{2\gamma bx_A}{b^2-v^2}\right)\right]$.

Finally, we obtain

$$\begin{aligned}
\phi_A^{+1}(x_0,-1) &= \phi_A^{-1}(x_0,-1) = \frac{\left(1-\frac{v}{b}\right)\exp\left(\frac{2\gamma b x_B}{b^2-v^2}\right)+\left(1+\frac{v}{b}\right)\exp\left(\frac{2\gamma b x_0}{b^2-v^2}\right)}{\left(1-\frac{v}{b}\right)\exp\left(\frac{2\gamma b x_B}{b^2-v^2}\right)+\left(1+\frac{v}{b}\right)\exp\left(\frac{2\gamma b x_A}{b^2-v^2}\right)},\\
\phi_A^{+1}(x_0,+1) &= \phi_A^{-1}(x_0,+1) = \frac{\left(1-\frac{v}{b}\right)\left[\exp\left(\frac{2\gamma b x_B}{b^2-v^2}\right)-\exp\left(\frac{2\gamma b x_0}{b^2-v^2}\right)\right]}{\left(1-\frac{v}{b}\right)\exp\left(\frac{2\gamma b x_B}{b^2-v^2}\right)+\left(1+\frac{v}{b}\right)\exp\left(\frac{2\gamma b x_A}{b^2-v^2}\right)},\\
\phi_B^{+1}(x_0,-1) &= \phi_B^{-1}(x_0,-1) = \frac{\left(1+\frac{v}{b}\right)\left[\exp\left(\frac{2\gamma b x_A}{b^2-v^2}\right)-\exp\left(\frac{2\gamma b x_0}{b^2-v^2}\right)\right]}{\left(1-\frac{v}{b}\right)\exp\left(\frac{2\gamma b x_B}{b^2-v^2}\right)+\left(1+\frac{v}{b}\right)\exp\left(\frac{2\gamma b x_A}{b^2-v^2}\right)},\\
\phi_B^{+1}(x_0,+1) &= \phi_B^{-1}(x_0,+1) = \frac{\left(1+\frac{v}{b}\right)\exp\left(\frac{2\gamma b x_A}{b^2-v^2}\right)+\left(1-\frac{v}{b}\right)\exp\left(\frac{2\gamma b x_0}{b^2-v^2}\right)}{\left(1-\frac{v}{b}\right)\exp\left(\frac{2\gamma b x_B}{b^2-v^2}\right)+\left(1+\frac{v}{b}\right)\exp\left(\frac{2\gamma b x_A}{b^2-v^2}\right)}.
\end{aligned} \tag{B9}$$

Then from Eq. (14) we derive

$$\begin{aligned}
&\phi_A(x_0,-1) = \phi_A^{+1}(x_0,-1), \phi_A(x_0,+1) = \phi_A^{+1}(x_0,+1),\\
&\phi_B(x_0,-1) = \phi_B^{+1}(x_0,-1), \phi_B(x_0,+1) = \phi_B^{+1}(x_0,+1),\\
&\phi_A(x_0) = \frac{\left(1-\frac{v}{b}\right)\exp\left(\frac{2\gamma b x_B}{b^2-v^2}\right)+\frac{v}{b}\exp\left(\frac{2\gamma b x_0}{b^2-v^2}\right)}{\left(1-\frac{v}{b}\right)\exp\left(\frac{2\gamma b x_B}{b^2-v^2}\right)+\left(1+\frac{v}{b}\right)\exp\left(\frac{2\gamma b x_A}{b^2-v^2}\right)},\\
&\phi_B(x_0) = \frac{\left(1+\frac{v}{b}\right)\exp\left(\frac{2\gamma b x_A}{b^2-v^2}\right)-\frac{v}{b}\exp\left(\frac{2\gamma b x_0}{b^2-v^2}\right)}{\left(1-\frac{v}{b}\right)\exp\left(\frac{2\gamma b x_B}{b^2-v^2}\right)+\left(1+\frac{v}{b}\right)\exp\left(\frac{2\gamma b x_A}{b^2-v^2}\right)}.
\end{aligned} \tag{B10}$$

Then, combining Eqs. (28) and (B10), we obtain the positional PDFs $p(x|\mathrm{NPF}_F)$ and $p(x|\mathrm{NPF}_R)$ for unproductive attempts in forward and reverse directions, respectively.

Appendix C: Detailed theoretical results of the mean transition path time, transition path shape and variation coefficient

According to Eq. (15), we define $\eta_A(x_0) = K^{(1)}(x_A|x_0,+1) + K^{(1)}(x_A|x_0,-1)$ and $\epsilon_A(x_0) = K^{(1)}(x_A|x_0,+1) - K^{(1)}(x_A|x_0,-1)$ and find that

$$\begin{aligned}
f(x_0)\frac{\partial}{\partial x_0}\eta_A(x_0) + v\frac{\partial}{\partial x_0}\epsilon_A(x_0) &= -\phi_A(x_0,+1) - \phi_A(x_0,-1),\\
f(x_0)\frac{\partial}{\partial x_0}\epsilon_A(x_0) + v\frac{\partial}{\partial x_0}\eta_A(x_0) &= \phi_A(x_0,-1) - \phi_A(x_0,+1) + 2\gamma\epsilon_A(x_0).
\end{aligned} \tag{C1}$$

With the help of the boundary conditions (6) we then get

$$\begin{aligned}
\epsilon_A(x_0) &= \mathscr{N}(x_0)M_1^{-1}(x_0),\\
\eta_A(x_0) &= 4\gamma v^2 C_3 \int_{x_A}^{x_0}\int_{x_A}^{x}[W(y)]^{-(\frac{\gamma}{2a}+1)}Q_1(y)dy[W(x)]^{\frac{\gamma}{2a}-1}dx\\
&\quad - 2\gamma v^2 C_4 \int_{x_A}^{x_0}\int_{x_A}^{x}[W(y)]^{-(\frac{\gamma}{2a}+1)}dy[W(x)]^{\frac{\gamma}{2a}-1}dx\\
&\quad + \frac{\gamma v}{2a}C_3\int_{x_A}^{x_0} log[M_2(x)][W(x)]^{\frac{\gamma}{2a}-1}dx - 2\gamma v D_5[W(x_B)]^{-\frac{\gamma}{2a}}\int_{x_A}^{x_0}[W(x)]^{\frac{\gamma}{2a}-1}dx\\
&\quad + C_3\int_{x_A}^{x_0}Q_1(x)\frac{2(2ax+b)}{(2ax+b)^2-v^2}dx - \frac{B}{4a}log[M_2(x_0)] + vC_3\int_{x_A}^{x_0}[W(x)]^{\frac{\gamma}{2a}-1}dx + D_6,\\
\mathscr{N}(x_0) &= -2n_0 v C_3\int_{x_A}^{x_0}[W(x)]^{-(\frac{\gamma}{2a}+1)}Q_1(x)dx + n_0 v C_4\int_{x_A}^{x_0}[W(x)]^{-(\frac{\gamma}{2a}+1)}dx\\
&\quad - \frac{n_0 C_3}{4a}log[M_2(x_0)] + D_5,
\end{aligned} \tag{C2}$$

where C_3 and C_4 are given below Eq. (11) and $n_0 = \left[(2ax_B+b)^2 - v^2\right]^{\frac{\gamma}{2a}}$ as well as $M_2(x_0) = \frac{(2ax_0+b)^2-v^2}{(2ax_A+b)^2-v^2}$, $W(x_0) = (2ax_0+b)^2 - v^2$, $Q_1(x_0) = \int_{x_A}^{x_0}\gamma v[W(x)]^{\frac{\gamma}{2a}-1}dx$, and $D_6 = D_5[M_2(x_B)]^{-\frac{\gamma}{2a}}$. D_5 can be obtained from $\eta_A(x_B) + \epsilon_A(x_B) = 0$.

Eq. (20) can be rewritten as

$$\begin{aligned}
\tau^{\mathrm{TP}}(x_B|x_A) &= \frac{K^{(1)}(x_B|x_A)}{\phi_B(x_A)} = \frac{D_2}{\phi_B(x_A)},\\
\tau^{\mathrm{TP}}(x_A|x_B) &= \frac{K^{(1)}(x_A|x_B)}{\phi_A(x_B)} = \frac{D_5}{\phi_A(x_B)}.
\end{aligned} \tag{C3}$$

For the linear potential case $f(x) = -U/2 = b$ ($a = 0$),

$$\begin{aligned}
G_1 &= -a_1 b_1 C_{11}(x_B - x_A) + b_2 C_{11}(a_1 - a_2),\\
G_2 &= b_3 C_{11}(n_2 - n_1 x_A) + b_4 n_1 C_{11} - a_2 b_5 C_{11}(x_B - x_A),\\
G_3 &= G_1 + b_7\left(\frac{a_1}{a_2} - 1\right), G_4 = G_2 - \frac{b_6 n_1}{a_2} - \frac{2}{b}(x_B - x_A),\\
G_5 &= -\frac{G_3 + G_4}{a_1 + a_2 - a_3 n_1}, G_6 = a_2 G_5,\\
G_7 &= G_4 - a_3 n_1 G_5 + G_6,\\
D_1 &= -\frac{(G_1 + G_2)}{2(a_1 + a_2 - a_3 n_1)},\\
D_2 &= a_2 D_1,\\
D_5 &= \frac{1}{2}G_7,
\end{aligned} \tag{C4}$$

where $a_0 = \frac{2\gamma b}{b^2-v^2}$, $a_1 = \exp(a_0 x_B)$, $a_2 = \exp(a_0 x_A)$, $a_3 = \frac{2\gamma v}{b^2-v^2}$, $b_1 = \frac{b^2+v^2}{b(b^2-v^2)}$, $b_2 = \frac{v(b+v)}{2\gamma b^2}$, $b_3 = \frac{2\gamma v(b^2+v^2)}{b(b^2-v^2)^2}$, $b_4 = \frac{2v}{b^2-v^2} - \frac{v^2}{b^2(b-v)}$, $b_5 = \frac{b+v}{b^2}$, $b_6 = \frac{2v^2}{b(b^2-v^2)}$, $b_7 = \frac{v}{\gamma b}$, $n_1 = \frac{a_1-a_2}{a_0}$, $n_2 = \frac{1}{a_0}(a_1 x_B - a_2 x_A - n_1)$, and C_{11} appears below Eq. (B6).

The final results based on Eq. (C3) then read

$$\begin{aligned}
\tau^{\rm TP}(x_B|x_A) =& \frac{\Big[-\frac{v}{\gamma b}+\frac{v^3}{\gamma b^3}+\frac{b^2+v^2}{b^2(b+v)}(x_B-x_A)\Big]\exp\left(\frac{2\gamma b x_B}{b^2-v^2}\right)+\Big[\frac{v}{\gamma b}-\frac{v^3}{\gamma b^3}+\frac{b+v}{b^2}(x_B-x_A)\Big]\exp\left(\frac{2\gamma b x_A}{b^2-v^2}\right)}{\left(1-\frac{v}{b}\right)\exp\left(\frac{2\gamma b x_B}{b^2-v^2}\right)+\left(1+\frac{v}{b}\right)\exp\left(\frac{2\gamma b x_A}{b^2-v^2}\right)},\\
\tau^{\rm TP}(x_A|x_B) =& \frac{\Big[-\frac{v}{\gamma b}+\frac{v^3}{\gamma b^3}-\frac{b-v}{b^2}(x_B-x_A)\Big]\exp\left(\frac{2\gamma b x_B}{b^2-v^2}\right)+\Big[\frac{v}{\gamma b}-\frac{v^3}{\gamma b^3}-\frac{b^2+v^2}{b^2(b+v)}(x_B-x_A)\Big]\exp\left(\frac{2\gamma b x_A}{b^2-v^2}\right)}{\left(1-\frac{v}{b}\right)\exp\left(\frac{2\gamma b x_B}{b^2-v^2}\right)+\left(1+\frac{v}{b}\right)\exp\left(\frac{2\gamma b x_A}{b^2-v^2}\right)},\\
\tau^{\rm TP}(x_A|x_B)-&\tau^{\rm TP}(x_B|x_A) = \frac{2b^2(x_B-x_A)\exp\left(\frac{2\gamma b x_B}{b^2-v^2}\right)+2(b^2+bv+v^2)(x_B-x_A)\exp\left(\frac{2\gamma b x_A}{b^2-v^2}\right)}{b^2(b+v)\left[\left(1-\frac{v}{b}\right)\exp\left(\frac{2\gamma b x_B}{b^2-v^2}\right)+\left(1+\frac{v}{b}\right)\exp\left(\frac{2\gamma b x_A}{b^2-v^2}\right)\right]}.
\end{aligned} \tag{C5}$$

Then,

$$\begin{aligned}
K^{(1)}(x_B|x_0) =& b_3C_{11}(n_4-x_An_3)+b_4C_{11}n_3-a_2b_5C_{11}(x_0-x_A)\\
&-a_3n_3D_1+D_2,\\
K^{(1)}(x_A|x_0) =& b_3C_{11}(n_4-x_An_3)+b_4C_{11}n_3-a_2b_5C_{11}(x_0-x_A)\\
&-\frac{1}{a_2}b_6n_3-\frac{2}{b}(x_0-x_A)-a_3n_3D_5+D_6,
\end{aligned} \tag{C6}$$

where $n_3=\frac{1}{a_0}\Big[\exp(a_0x_0)-a_2\Big]$, $n_4=\frac{1}{a_0}\Big[x_0\exp(a_0x_0)-x_Aa_2-n_3\Big]$.

We define $\omega_A(x_0)=K^{(2)}(x_A|x_0,+1)+K^{(2)}(x_A|x_0,-1)$ and $\theta_A(x_0)=K^{(2)}(x_A|x_0,+1)-K^{(2)}(x_A|x_0,-1)$. Then Eq. (23) can be rewritten as

$$\begin{aligned}
f(x_0)\frac{\partial}{\partial x_0}\omega_A(x_0)+v\frac{\partial}{\partial x_0}\theta_A(x_0) =& -2K^{(1)}(x_A|x_0,+1)-2K^{(1)}(x_A|x_0,-1),\\
f(x_0)\frac{\partial}{\partial x_0}\theta_A(x_0)+v\frac{\partial}{\partial x_0}\omega_A(x_0) =& 2\gamma\theta_A(x_0)+2\Big[K^{(1)}(x_A|x_0,-1)-K^{(1)}(x_A|x_0,+1)\Big].
\end{aligned} \tag{C7}$$

This leads us to

$$\begin{aligned}
\theta_A(x_0) =& \frac{2}{M_1(x_0)}\int_{x_A}^{x_0}\frac{M_1(x)K^{(1)}(x_A|x,-1)}{f(x)-v}dx-\frac{2}{M_1(x_0)}\int_{x_A}^{x_0}\frac{M_1(x)K^{(1)}(x_A|x,+1)}{f(x)+v}dx+\frac{D_7}{M_1(x_0)},\\
\omega_A(x_0) =& -2\int_{x_A}^{x_0}\frac{K^{(1)}(x_A|x,-1)}{f(x)-v}dx-4\gamma v\int_{x_A}^{x_0}\int_{x_A}^{x}\frac{M_1(y)K^{(1)}(x_A|x,-1)}{f(y)-v}dy\frac{dx}{M_1(x)(f^2(x)-v^2)}\\
&-2\int_{x_A}^{x_0}\frac{K^{(1)}(x_A|x,+1)}{f(x)+v}dx+4\gamma v\int_{x_A}^{x_0}\int_{x_A}^{x}\frac{M_1(y)K^{(1)}(x_A|x,+1)}{f(y)+v}dy\frac{dx}{M_1(x)(f^2(x)-v^2)}\\
&-2\gamma vD_7\int_{x_A}^{x_0}\frac{dx}{M_1(x)(f^2(x)-v^2)}+D_8,
\end{aligned} \tag{C8}$$

where $D_8=\frac{D_7}{M_1(x_A)}$, D_7 can be derived from $\theta_A(x_B)+\omega_A(x_B)=0$, and $M_1(x_0)$ appears under Eq. (18).

Similarly, for the linear potential case $f(x)=-U/2=b$ ($a=0$), we present the simplest forms of the second moment of the forward transition path time, $\langle t_{\rm TP}^2\rangle=K^{(2)}(x_B|x_A)/\phi_B(x_A)$ and COV C_V of the forward transition path time distribution,

$$\begin{aligned}
\langle t_{\rm TP}^2\rangle =& -\frac{(x_B-x_A)^2T_1+(x_B-x_A)T_2+T_3}{2\left[(1-\frac{v}{b})a_1+(1+\frac{v}{b})a_2\right]^2},\\
C_V =& \frac{\left[(x_B-x_A)^2T_4+(x_B-x_A)T_5+T_6\right]^{1/2}}{\left[m_1+m_2(x_B-x_A)\right]a_1+\left[-m_1+m_3(x_B-x_A)\right]a_2},\\
T_1 =& E_1a_1^2+E_2a_1a_2+E_6a_2^2, T_2=E_9a_1^2+E_4a_1a_2+E_7a_2^2,\\
T_3 =& E_3a_1^2+E_5a_1a_2+E_8a_2^2, T_4=s_1a_1a_2,\\
T_5 =& s_7a_1^2+s_3a_1a_2+s_5a_2^2, T_6=s_2a_1^2+s_4a_1a_2+s_6a_2^2,
\end{aligned} \tag{C9}$$

where

$$
\begin{aligned}
&E_1 = -\frac{2(b^2+v^2)^2}{b^4(b+v)^2}, E_2 = \frac{4(3v^4-b^4)}{b^4(b^2-v^2)},\\
&E_3 = \frac{v^2(b^2-v^2)(6bv-4b^2-2v^2)}{\gamma^2 b^6}, E_4 = \frac{8v^2(b^2-3bv)}{\gamma b^5},\\
&E_5 = \frac{4v^2(2b^4-b^2v^2-v^4)}{\gamma^2 b^6}, E_6 = \frac{-2(b+v)^2}{b^4},\\
&E_7 = \frac{2v^4-6b^2v^2-4b^3v}{\gamma b^5}, E_8 = \frac{-2v^2(b^2-v^2)(2b^2+3bv+v^2)}{\gamma^2 b^6},\\
&E_9 = \frac{2v(b-v)(2b^2+bv+v^2)}{\gamma b^5},\\
&s_1 = -\frac{4v^4}{b^4(b^2-v^2)}, s_2 = \frac{(b^2-v^2)(2v^4+b^2v^2-3bv^3)}{\gamma^2 b^6}, s_3 = \frac{8v^3}{\gamma b^4},\\
&s_4 = -\frac{2v^2(b^2-v^2)(b^2+2v^2)}{\gamma^2 b^6}, s_5 = \frac{v(2bv^2+b^2v+v^3)}{\gamma^2 b^5},\\
&s_6 = \frac{(b^2-v^2)(b^2v^2+2v^4+3bv^3)}{\gamma^2 b^6}, s_7 = -\frac{(b-v)^2v^2}{\gamma b^5},\\
&m_1 = -\frac{v(b^2-v^2)}{\gamma b^3}, m_2 = \frac{b^2+v^2}{b^2(b+v)},\\
&m_3 = \frac{b+v}{b^2},
\end{aligned}
\tag{C10}
$$

and a_1, a_2 were presented below Eq. (C4).

Appendix D: Explicit reselts of Eq. (30)

Here, we present some resluts of the mean return times $\tau_R(x_A \to x_A)$ and $\tau_R(x_B \to x_B)$, for the linear potential case. Then, Eq. (30) could be rewritten as

$$
\begin{aligned}
\tau_R(x_A \to x_A) &= \frac{(v^3-b^2v)\exp\left(\frac{4\gamma b x_A}{b^2-v^2}\right) + \left[2bv(b-v) - \frac{4\gamma b v^2(x_B-x_A)}{b+v}\right]\exp\left(\frac{2\gamma b(x_B+x_A)}{b^2-v^2}\right) - v(b-v)^2\exp\left(\frac{4\gamma b x_B}{b^2-v^2}\right)}{2\gamma b\left[v(b+v)\exp\left(\frac{4\gamma b x_A}{b^2-v^2}\right) + (b-v)(b+2v)\exp\left(\frac{2\gamma b(x_B+x_A)}{b^2-v^2}\right) + (b-v)^2\exp\left(\frac{4\gamma b x_B}{b^2-v^2}\right)\right]},\\
\tau_R(x_B \to x_B) &= \frac{v(b+v)^2\exp\left(\frac{4\gamma b x_A}{b^2-v^2}\right) - \left[2bv(b+v) - \frac{4\gamma b v^2(x_B-x_A)}{b-v}\right]\exp\left(\frac{2\gamma b(x_B+x_A)}{b^2-v^2}\right) - (v^3-b^2v)\exp\left(\frac{4\gamma b x_B}{b^2-v^2}\right)}{2\gamma b\left[(b+v)^2\exp\left(\frac{4\gamma b x_A}{b^2-v^2}\right) + (b+v)(b-2v)\exp\left(\frac{2\gamma b(x_B+x_A)}{b^2-v^2}\right) - v(b-v)\exp\left(\frac{4\gamma b x_B}{b^2-v^2}\right)\right]}.
\end{aligned}
\tag{D1}
$$

[1] L. Tröger, F. Goirand, K. Alim. Size-dependent self-avoidance enables superdiffusive migration in macroscopic unicellulars. Proc. Natl. Acad. SCI. USA, 2024, **121**(13): e2312611121.
[2] S. Riedel, L.A. Hoffmann, L. Giomi, et al. Designing highly efficient interlocking interactions in anisotropic active particles. Nat. Commun., 2024, **15**(1): 5692.
[3] C. Bechinger, R. Di Leonardo, H. Löwen, C. Reichhardt, G. Volpe, and G. Volpe. Active particles in complex and crowded environments. Rev. Mod. Phys., 2016, **88**: 045006.
[4] M. C. Marchetti, J. F. Joanny, S. Ramaswamy, T. B. Liverpool, J. Prost, M. Rao, and R. Aditi Simha. Hydrodynamics of soft active matter. Rev. Mod. Phys., 2013, **85**: 1143.
[5] Y. Hatwalne, S. Ramaswamy, M. Rao, et al. Rheology of active-particle suspensions. Phys. Rev. Lett., 2004, **92**(11): 118101.
[6] T. Vicsek, A. Zafeiris. Collective motion. Phys. Rep., 2012, **517**(3-4): 71-140.
[7] P. Pietzonka, E. Fodor, C. Lohrmann, et al. Autonomous engines driven by active matter: Energetics and design principles. Phys. Rev. X, 2019, **9**(4): 041032.

[8] T. Sanchez, D.T.N. Chen, S.J. DeCamp, et al. Spontaneous motion in hierarchically assembled active matter. Nature, 2012, **491**(7424): 431-434.
[9] G. Gardi, S. Ceron, W. Wang, et al. Microrobot collectives with reconfigurable morphologies, behaviors, and functions. Nat. Commun., 2022, **13**(1): 2239.
[10] M. Yang, Y. Zhang, F. Mou, et al. Swarming magnetic nanorobots bio-interfaced by heparinoid-polymer brushes for in vivo safe synergistic thrombolysis. Sci. Adv., 2023, **9**(48): eadk7251.
[11] S. Palagi, P. Fischer. Bioinspired microrobots. Nat. Rev. Mater., 2018, **3**(6): 113-124.
[12] P. Gottheil, J. Lippoldt, S. Grosser, et al. State of cell unjamming correlates with distant metastasis in cancer patients. Phys. Rev. X, 2023, **13**(3): 031003.
[13] C. Kurzthaler, Y. Zhao, N. Zhou, et al. Characterization and control of the run-and-tumble dynamics of Escherichia Coli. Phys. Rev. Lett., 2024, **132**(3): 038302.
[14] T. Mano, J.B. Delfau, J. Iwasawa, et al. Optimal run-and-tumble-based transportation of a Janus particle with active steering. Proc. Natl. Acad. SCI. USA, 2017, **114**(13): E2580-E2589.
[15] S. Johnson, B. Freedman, J.X. Tang. Run-and-tumble kinematics of Enterobacter Sp. SM3. Phys. Rev. E, 2024, **109**(6): 064402.
[16] T. Bertrand, Y. Zhao, O. Bénichou, et al. Optimized diffusion of run-and-tumble particles in crowded environments. Phys. Rev. Lett., 2018, **120**(19): 198103.
[17] I. Santra, U. Basu, S. Sabhapandit. Universal framework for the long-time position distribution of free active particles. J. Phys. A-Math. Theor., 2022, **55**(38): 385002.
[18] P. Singh, S. Santra, A. Kundu. Extremal statistics of a one-dimensional run and tumble particle with an absorbing wall. J. Phys. A-Math. Theor., 2022, **55**(46): 465004.
[19] D.S. Dean, S.N. Majumdar, H. Schawe. Position distribution in a generalized run-and-tumble process. Phys. Rev. E, 2021, **103**(1): 012130.
[20] G. Gradenigo, S.N. Majumdar. A first-order dynamical transition in the displacement distribution of a driven run-and-tumble particle. J. Stat. Mech.-Theory E., 2019, **2019**(5): 053206.
[21] L. Angelani. One-dimensional run-and-tumble motions with generic boundary conditions. J. Phys. A-Math. Theor., 2023, **2019**(45): 455003.
[22] G. Tucci, A. Gambassi, S.N. Majumdar, et al. First-passage time of run-and-tumble particles with noninstantaneous resetting. Phys. Rev. E, 2022, **106**(4): 044127.
[23] K. Malakar, V. Jemseena, A. Kundu, et al. Steady state, relaxation and first-passage properties of a run-and-tumble particle in one-dimension. J. Stat. Mech.-Theory E., 2018, **2018**(4): 043215.
[24] P. Singh, A. Kundu. Generalised 'Arcsine' laws for run-and-tumble particle in one dimension. J. Stat. Mech.-Theory E., 2019, **2019**(845): 083205.
[25] W.R. DiLuzio, L. Turner, M. Mayer, et al. Escherichia coli swim on the right-hand side. Nature, 2005, **435**(7046): 1271-1274.
[26] C.D. Chin, V. Linder, S.K. Sia. Lab-on-a-chip devices for global health: Past studies and future opportunities. Lab Chip, 2007, **7**(1): 41-57.
[27] F.J. Sevilla, A.V. Arzola, E.P. Cital. Stationary superstatistics distributions of trapped run-and-tumble particles. Phys. Rev. E, 2019, **99**(1): 012145.
[28] N.R. Smith, P. Le Doussal, S.N. Majumdar, et al. Exact position distribution of a harmonically confined run-and-tumble particle in two dimensions. Phys. Rev. E, 2022, **106**(5): 054133.
[29] U. Basu, S.N. Majumdar, A. Rosso, et al. Exact stationary state of a run-and-tumble particle with three internal states in a harmonic trap. J. Phys. A-Math. Theor., 2020, **53**(9): 09LT01.
[30] D. Frydel. Run-and-tumble oscillator: Moment analysis of stationary distributions. Phys. Fluids, 2023, **35**(10).
[31] N.R. Smith, P. Le Doussal, S.N. Majumdar, et al. Exact position distribution of a harmonically confined run-and-tumble particle in two dimensions. Phys. Rev. E, 2022, **106**(5): 054133.
[32] R. Garcia-Millan, G. Pruessner. Run-and-tumble motion in a harmonic potential: Field theory and entropy production. J. Stat. Mech.-Theory E., 2021, **2021**(6): 063203.
[33] M. Paoluzzi, A. Puglisi, L. Angelani. Entropy production of run-and-tumble particles. Entropy, 2024, **26**(6): 443.
[34] P. Padmanabha, D.M. Busiello, A. Maritan, et al. Fluctuations of entropy production of a run-and-tumble particle. Phys. Rev. E, 2023, **107**(1): 014129.
[35] E. Jeon, B.G. Go, Y.W. Kim. Searching for a partially absorbing target by a run-and-tumble particle in a confined space. Phys. Rev. E, 2024, **109**(1): 014103.
[36] M. Guéneau, L. Touzo. Relating absorbing and hard wall boundary conditions for a one-dimensional run-and-tumble particle. J. Phys. A-Math. Theor., 2024, **57**(22): 225005.
[37] C. Roberts, Z. Zhen. Run-and-tumble motion in a linear ratchet potential: Analytic solution, power extraction, and first-passage properties. Phys. Rev. E, 2023, **108**(1): 014139.
[38] A. Dhar, A. Kundu, S.N. Majumdar, et al. Run-and-tumble particle in one-dimensional confining potentials: Steady-state, relaxation, and first-passage properties. Phys. Rev. E, 2019, **99**(3): 032132.
[39] F. Mori, P. Le Doussal, S.N. Majumdar, et al. Universal survival probability for a d-dimensional run-and-tumble particle. Phys. Rev. Lett., 2020, **124**(9): 090603.
[40] O. Farago, N.R. Smith. Confined run-and-tumble particles with non-Markovian tumbling statistics. Phys. Rev. E, 2024, **109**(4): 044121.
[41] N.R. Smith. Nonequilibrium steady state of trapped active particles. Phys. Rev. E, 2023, **108**(2): L022602.

[42] G. Li, J.X. Tang. Accumulation of microswimmers near a surface mediated by collision and rotational Brownian motion. Phys. Rev. Lett., 2009, **103**(7): 078101.
[43] T. Vojta, S. Halladay, S. Skinner, S. Janušonis, T. Guggenberger, and R. Metzler. Reflected fractional Brownian motion in one and higher dimensions. Phys. Rev. E, 2020, **102**: 032108.
[44] P. Hänggi, P. Talkner, M. Borkovec. Reaction-rate theory: Fifty years after Kramers. Rev. Mod. Phys., 1990, **62**(2): 251.
[45] Y. Xu, H. Li, H.Y. Wang, et al. The estimates of the mean first exit time of a bistable system excited by Poisson white noise. J. Appl. Mech. Trans. ASME, 2017, **84**(9): 091004.
[46] G. Hummer, From transition paths to transition states and rate coefficients. J. Chem. Phys., 2004, **120**(2): 516-523.
[47] K. Neupane, F. Wang, M.T. Woodside. Direct measurement of sequence-dependent transition path times and conformational diffusion in DNA duplex formation. Biophys. J., 2017, **114**(6): 1329-1334.
[48] R. Satija, A.M. Berezhkovskii, D.E. Makarov. Broad distributions of transition-path times are fingerprints of multidimensionality of the underlying free energy landscapes. Proc. Natl. Acad. SCI. USA, 2020, **117**(44): 27116-27123.
[49] W.K. Kim and R.R. Netz. The mean shape of transition and first-passage paths. J. Chem. Phys., 2015, **143**(22): 224108.
[50] E. Pollak. Transition path time distribution, tunneling times, friction, and uncertainty. Phys. Rev. Lett., 2017, **118**(7): 070401.
[51] D.K. Lubensky, D.R. Nelson. Driven polymer translocation through a narrow pore. Biophys. J., 1999, **77**(4): 1824-1838.
[52] W.M. Jacobs, E.I. Shakhnovich. Accurate protein-folding transition-path statistics from a simple free-energy landscape. J. Phys. Chem. B, 2018, **122**(49): 11126-11136.
[53] H.S. Chung, I.V. Gopich, K. Mchale, et al. Photon-by-photon analysis of single molecule uorescence trajectories determines an upper bound for the transition path time in protein folding. Biophys. J., 2011, **100**(3): 349a.
[54] V. Da Costa, Y. Henry, F. Bardou, et al. Experimental evidence and consequences of rare events in quantum tunneling. Eur. Phys. J. B, 2000, **13**(2): 297-303.
[55] W. Sung, P.J. Park. Polymer translocation through a pore in a membrane. Phys. Rev. Lett., 1996, **77**(4): 783.
[56] D.E. Makarov. Shapes of dominant transition paths from single-molecule force spectroscopy. J. Chem. Phys., 2015, **143**(19): 194103.
[57] A.M. Berezhkovskii, D.E. Makarov. On distributions of barrier crossing times as observed in single-molecule studies of biomolecules. Biophys. Rep., 2021, **1**(2): 100029.
[58] H. Li, Y. Xu, R. Metzler, et al. Transition path properties for one-dimensional non-Markovian models. J. Phys. A-Math. Theor., 2024, **57**(35): 355201.
[59] A. Lyons, A. Devi, N.Q. Hoffer, et al. Quantifying the properties of nonproductive attempts at thermally activated energy-barrier crossing through direct observation. Phys. Rev. X, 2024, **14**(1): 011017.
[60] D.E. Makarov. Failed barrier crossings tell a story. Physics, 2024, **17**: 25.
[61] H.S. Chung, K. McHale, J.M. Louis, et al. Single-molecule fluorescence experiments determine protein folding transition path times. Science, 2012, **335**(6071): 981-984.
[62] J. Stigler, F. Ziegler, A. Gieseke, J. C. M. Gebhardt, and M. Rief. The complex folding network of single calmodulin molecules. Science, 2011, **334**: 512.
[63] R. Tapia-Rojo, M. Mora, S. Board, J. Walker, R. Boujemaa-Paterski, O. Medalia, and S. Garcia-Manyes. Enhanced statistical sampling reveals microscopic complexity in the talin mechanosensor folding energy landscape. Nat. Phys., 2023, **19**: 52.
[64] N.Q. Hoffer, M.T. Woodside. Probing microscopic conformational dynamics in folding reactions by measuring transition paths. Curr. Opin. Chem. Biol., 2019, **53**: 68-74.
[65] F. Chiti, C.M. Dobson. Protein misfolding, functional amyloid, and human disease. Annu. Rev. Biochem., 2006, **75**(1): 333-366.
[66] C.M. Dobson. Protein misfolding, evolution and disease. Trends Biochem. SCI., 1999, **24**(9): 329-332.
[67] B.W. Zhang, D. Jasnow, D. M. Zuckerman. Transition-event durations in one-dimensional activated processes. J. Chem. Phys., 2007, **126**(7): 17970.
[68] R.J. Allen, D. Frenkel, P.R. ten Wolde. Simulating rare events in equilibrium or nonequilibrium stochastic systems. J. Chem. Phys., 2006, **124**(2): 024102.
[69] X.L. Wang, J. Feng, Y. Xu, et al. Deep learning-based state prediction of the Lorenz system with control parameters. Chaos, 2024, **34**(3): 033108.
[70] H. Li, Y. Xu, R. Metzler, J. Shen, and K. Suleiman, Transition path dynamics for one-dimensional run and tumble particle. Chaos, 2025, **35**(5): 053132.
[71] J. Gladrow, M. Ribezzi-Crivellari, F. Ritort, U. F. Keyser. Experimental evidence of symmetry breaking of transition-path times, Nat. Commun., 2019 **10**(1): 55.
[72] M. Guéneau, S. N. Majumdar, G. Schehr. Run-and-tumble particle in one-dimensional potentials: mean first-passage time and applications. Phys. Rev. E, 2025, **111**(1): 014144.

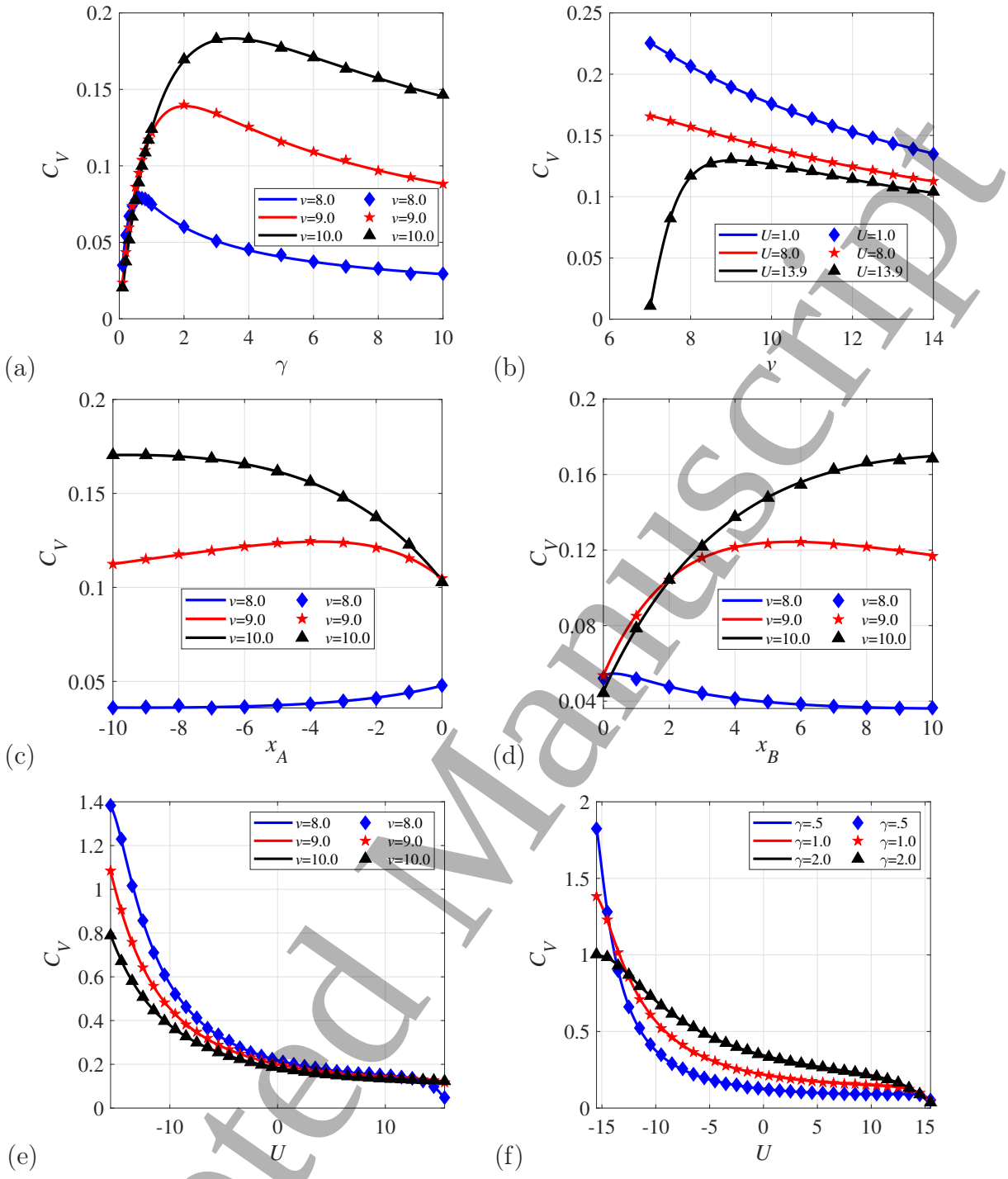

FIG. 7: COV C_V for the linear potential $V(x) = Ux/2$. (a) C_V for $U = 15$ and various v as function of γ, with $x_A = -1$ and $x_B = 3$. (b) C_V for different U as function of v for $\gamma = 1.0$, $x_A = -1$, and$x_B = 3$. (c) C_V as function of x_A for various v, with $U = 15.5$, $\gamma = 1.0$, and $x_B = 3$. (d) C_V as function of x_B for $U = 13.9$, $\gamma = 1.0$, and $x_A = -1$. (e) and (f) C_V as function of U for various v and γ, respectively, with $\gamma = 1.0$ (panel (e)) and$v = 9.0$ (panel (f)), with $x_A = -1$, and $x_B = 3$. The results of the simulations (symbols) are in excellent agreement with the theoretical results Eq. (C9) shown by the solid lines.

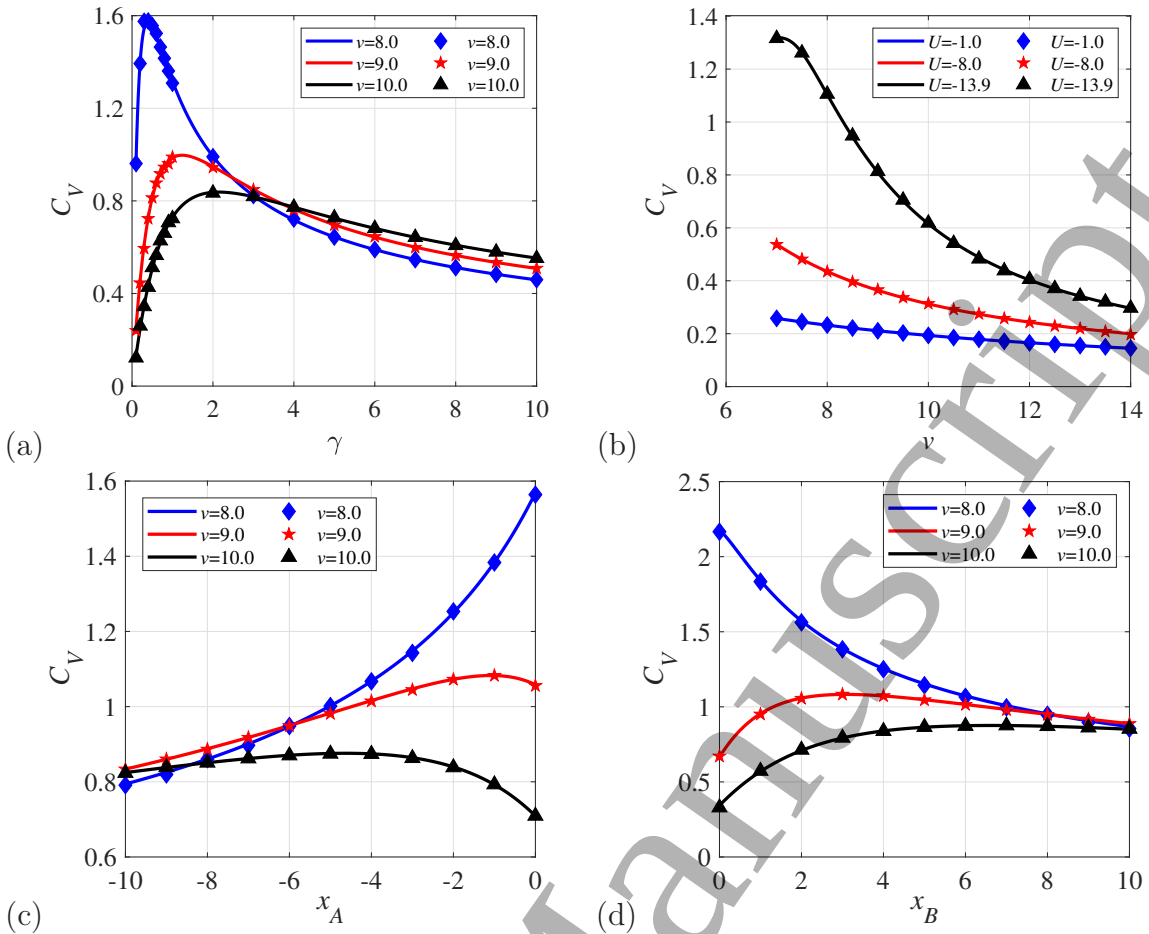

FIG. 8: COV C_V for the linear potential $V(x) = Ux/2$, with $U < 0$. (a) C_V for various v and $U = -15$ as function of γ, with $x_A = -1$ and $x_B = 3$. (b) C_V as function of v for different values of U and $\gamma = 1.0$, $x_A = -1$, $x_B = 3$. (c) C_V as function of x_A with $U = -15.5$, $\gamma = 1.0$, and $x_B = 3$. (d) C_V as function of x_B for $U = -13.9$, $\gamma = 1.0$, and $x_A = -1$. Excellent agreement is observed between the Monte Carlo simulations (symbols) and the analytical predictions (solid lines) from Eq. (C9).

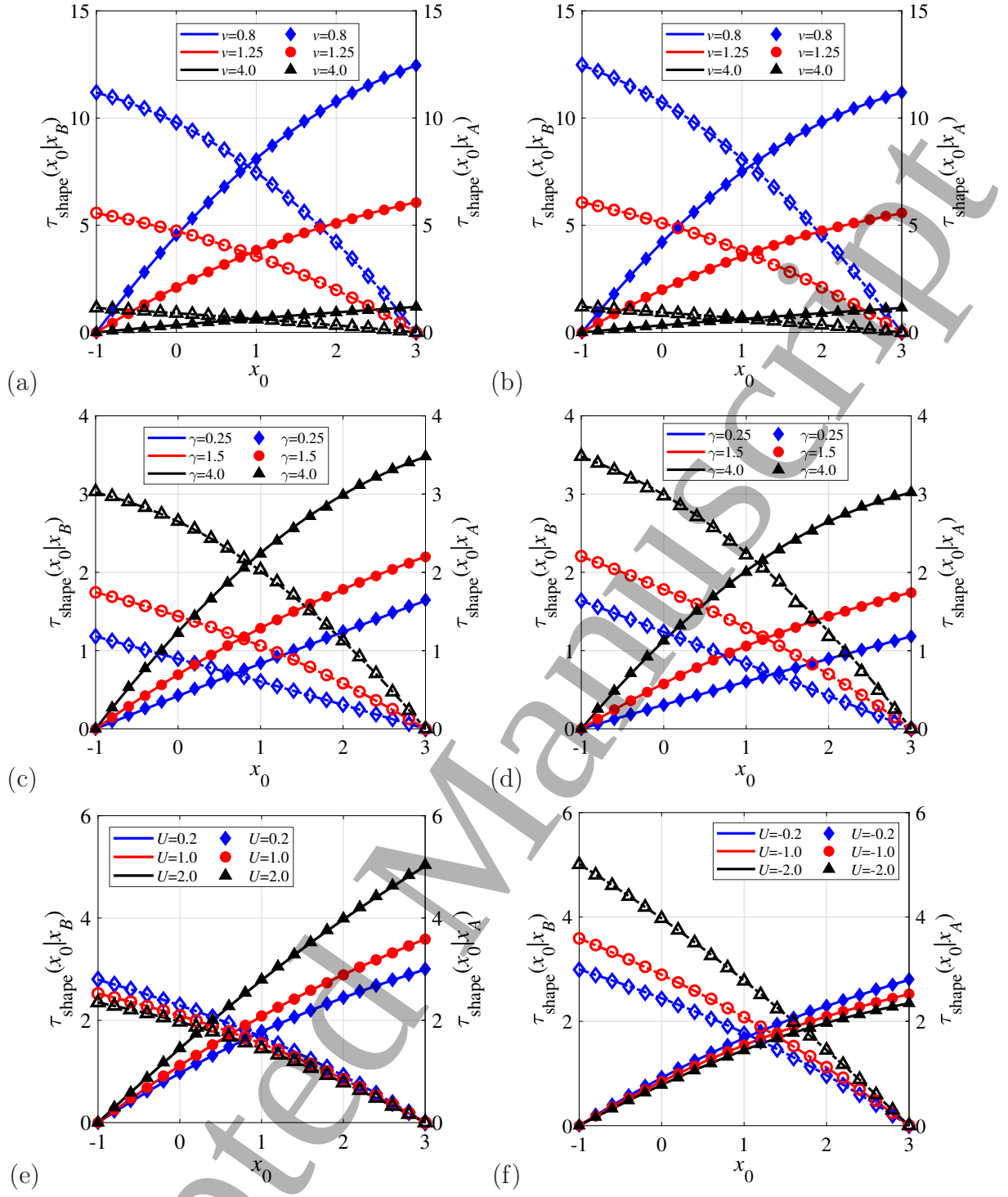

FIG. 9: Transition path shapes $\tau^{\rm TP}_{\rm shape}(x_0|x_A)$ and $\tau^{\rm TP}_{\rm shape}(x_0|x_B)$ as function of x_0 from Monte Carlo simulations (symbols) and for analytical results, Eq. (20). Open symbols are $\tau^{\rm TP}_{\rm shape}(x_0|x_A)$, the closed symbols stand for $\tau^{\rm TP}_{\rm shape}(x_0|x_B)$. The transition region is $[-1,3]$. Parameters: (a) $U=0.2$, $\gamma=1.0$. (b) $U=-0.2$, $\gamma=1.0$. (c) $U=1.0$, $v=3.0$. (d) $U=-1.0$, $v=3.0$. (e) $\gamma=1.0$, $v=2.0$. (f) $\gamma=1.0$, $v=2.0$. Note the different y-axes in panels (e,f). The theoretical results from Eq. (27) are in excellent agreement with the simulations.

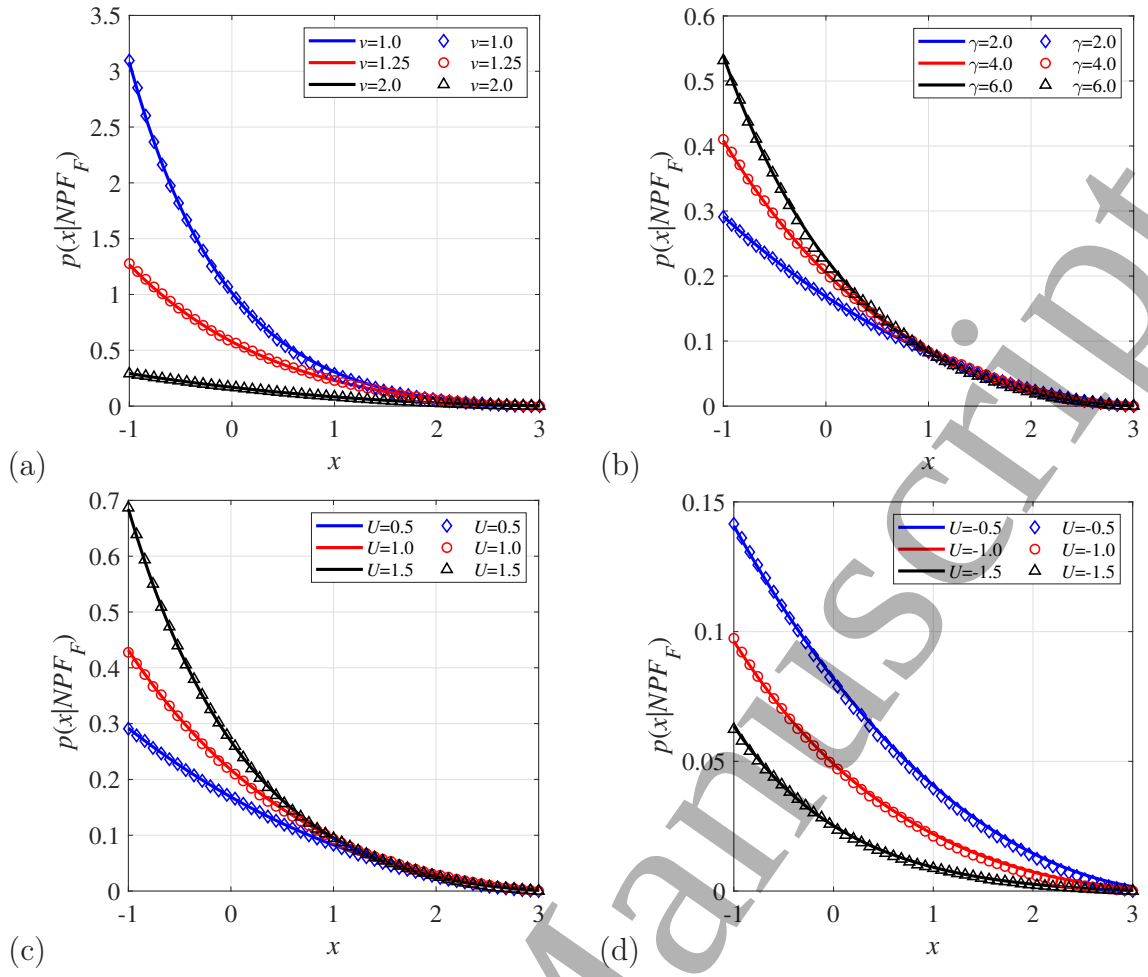

FIG. 10: Position distributions $p(x|\mathrm{NPF}_F)$ of forward unproductive attempts. Parameters: (a) $U = 0.5$, $\gamma = 2.0$. (b) $U = 0.5$, $v = 2.0$. (c) $\gamma = 2.0$, $v = 2.0$. (d) $\gamma = 2.0$, $v = 2.0$. Solid lines represent Eqs. (28) and (B10), the symbols show results of numerical simulations.

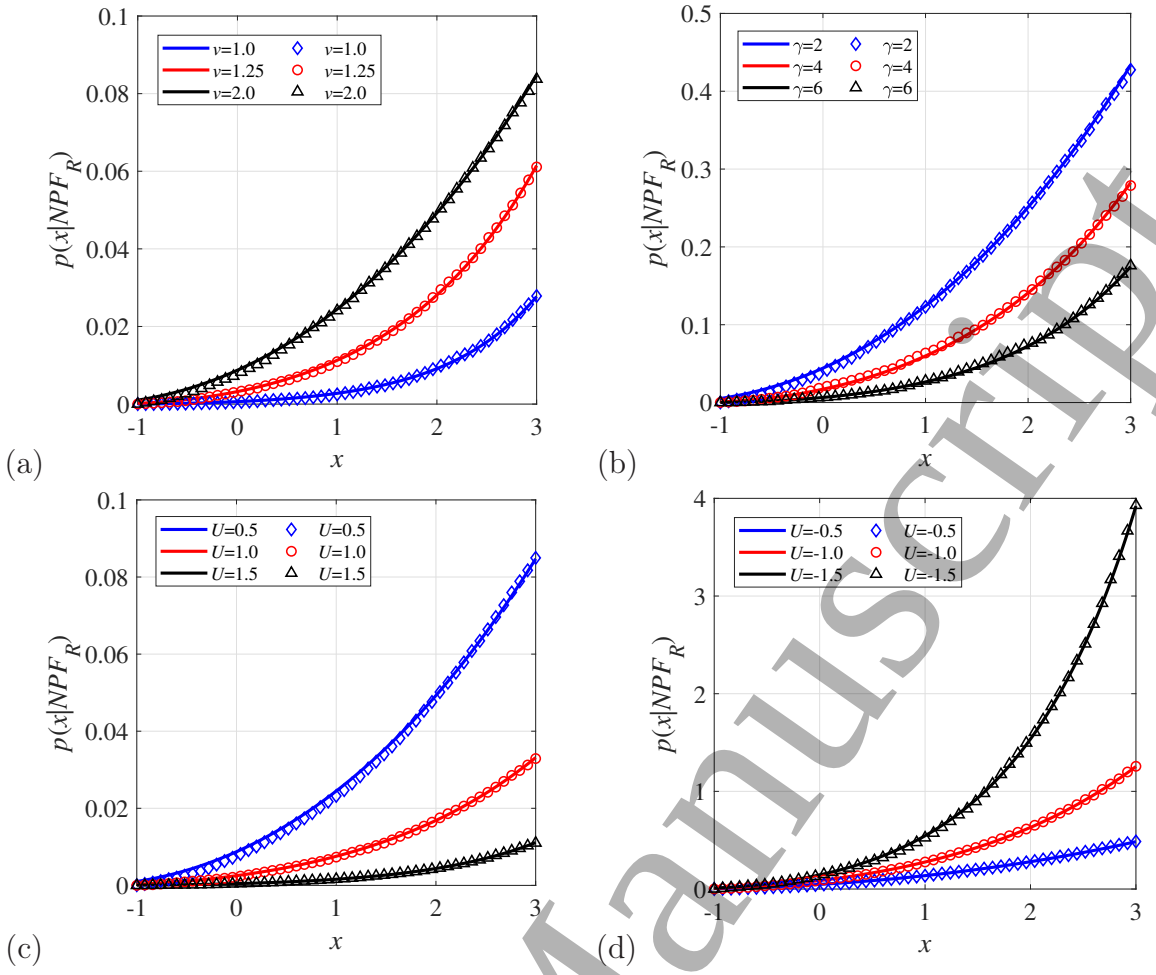

FIG. 11: Position distributions $p(x|\mathrm{NPF}_R)$ of reverse unproductive attempts. Parameters: (a) $U = 0.5$, $\gamma = 2.0$. (b) $U = 0.5$, $v = 2.0$. (c) $\gamma = 2.0$, $v = 2.0$. (d) $\gamma = 2.0$, $v = 2.0$. Solid lines represent Eqs. (28) and (B10), the symbols show results of numerical simulations.

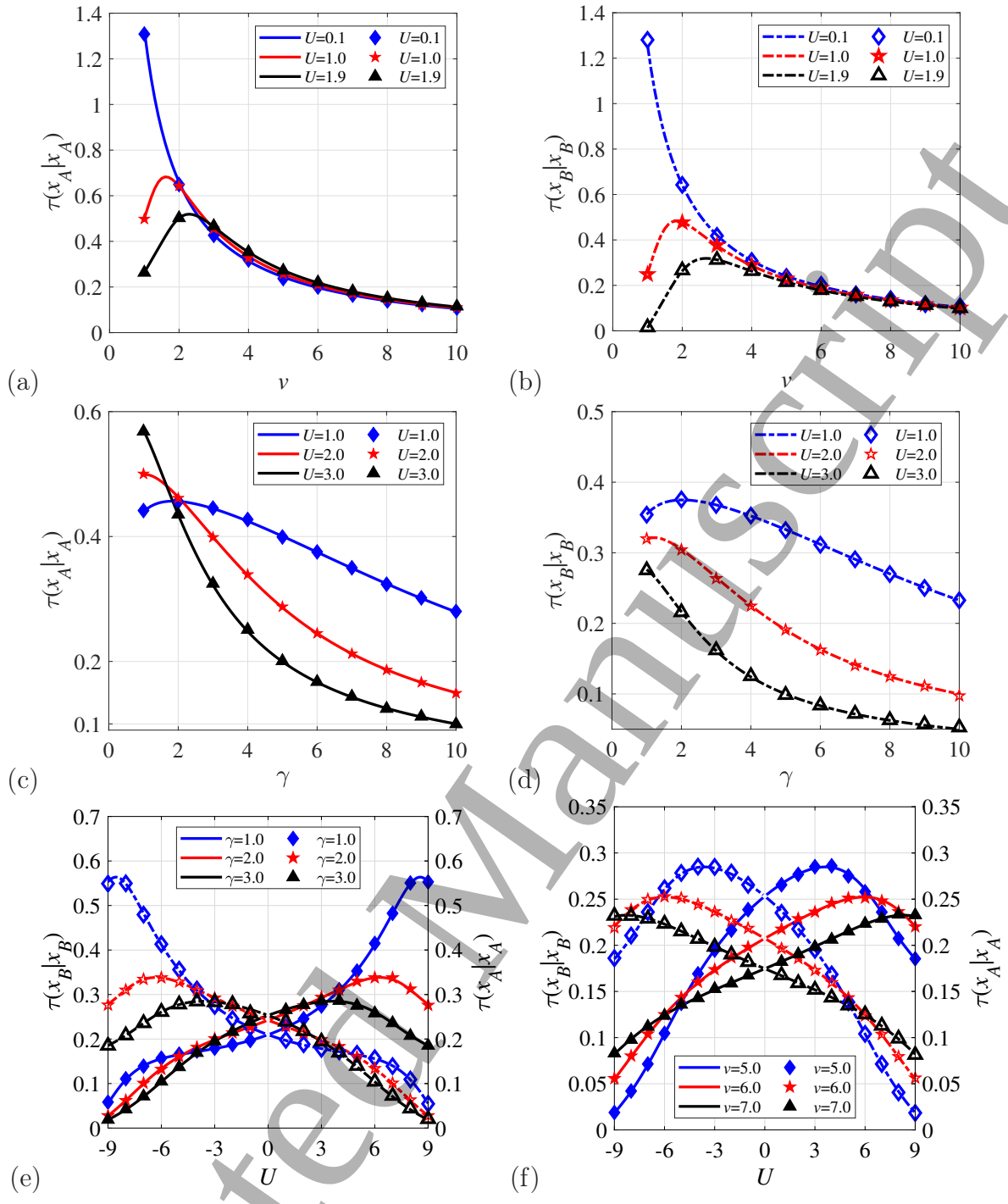

FIG. 12: Mean duration of forward and reverse unproductive attempts for the transition path region $[-1, 3]$. Parameters: (a,b) $\gamma = 2.0$. (c,d) $v = 3.0$. (e) $v = 5.0$. (f) $\gamma = 3.0$. Note the two different y-axes in panels (e,f). Solid and dashed lines represent the theoretical predictions for $\tau(x_A|x_A)$, $\tau(x_B|x_B)$ from Eq. (D1), respectively. The symbols represent numerical simulations.